

Leveraging the sampling efficiency of RE-EDS in OpenMM using a shifted reaction-field with an atom-based cutoff

Cite as: J. Chem. Phys. **157**, 104117 (2022); <https://doi.org/10.1063/5.0107935>

Submitted: 07 July 2022 • Accepted: 11 August 2022 • Accepted Manuscript Online: 11 August 2022 • Published Online: 13 September 2022

 Salomé R. Rieder,  Benjamin Ries,  Alžbeta Kubincová, et al.



[View Online](#)



[Export Citation](#)



[CrossMark](#)

ARTICLES YOU MAY BE INTERESTED IN

Machine learning implicit solvation for molecular dynamics

The Journal of Chemical Physics **155**, 084101 (2021); <https://doi.org/10.1063/5.0059915>

Molecular dipole moment learning via rotationally equivariant derivative kernels in molecular-orbital-based machine learning

The Journal of Chemical Physics **157**, 104109 (2022); <https://doi.org/10.1063/5.0101280>

Facilitating ab initio configurational sampling of multicomponent solids using an on-lattice neural network model and active learning

The Journal of Chemical Physics **157**, 104114 (2022); <https://doi.org/10.1063/5.0096645>

Time to get excited.
Lock-in Amplifiers – from DC to 8.5 GHz

[Find out more](#)

Zurich
Instruments

Leveraging the sampling efficiency of RE-EDS in OpenMM using a shifted reaction-field with an atom-based cutoff

Cite as: J. Chem. Phys. 157, 104117 (2022); doi: 10.1063/5.0107935

Submitted: 7 July 2022 • Accepted: 11 August 2022 •

Published Online: 13 September 2022



Salomé R. Rieder, Benjamin Ries, Alžbeta Kubincová, Candide Champion, Emilia P. Barros, Philippe H. Hünenberger, ^{a)} and Sereina Riniker^{b)}

AFFILIATIONS

Laboratory of Physical Chemistry, ETH Zürich, Vladimir-Prelog-Weg 2, 8093 Zürich, Switzerland

^{a)}Electronic mail: phil@igc.phys.chem.ethz.ch

^{b)}Author to whom correspondence should be addressed: sriniker@ethz.ch

ABSTRACT

Replica-exchange enveloping distribution sampling (RE-EDS) is a pathway-independent multistate free-energy method currently implemented in the GROMOS software package for molecular dynamics (MD) simulations. It has a high intrinsic sampling efficiency as the interactions between the unperturbed particles have to be calculated only once for multiple end-states. As a result, RE-EDS is an attractive method for the calculation of relative solvation and binding free energies. An essential requirement for reaching this high efficiency is the separability of the nonbonded interactions into solute–solute, solute–environment, and environment–environment contributions. Such a partitioning is trivial when using a Coulomb term with a reaction-field (RF) correction to model the electrostatic interactions but not when using lattice-sum schemes. To avoid cutoff artifacts, the RF correction is typically used in combination with a charge-group-based cutoff, which is not supported by most small-molecule force fields as well as other MD engines. To address this issue, we investigate the combination of RE-EDS simulations with a recently introduced RF scheme including a shifting function that enables the rigorous calculation of RF electrostatics with atom-based cutoffs. The resulting approach is validated by calculating solvation free energies with the generalized AMBER force field in water and chloroform using both the GROMOS software package and a proof-of-concept implementation in OpenMM.

© 2022 Author(s). All article content, except where otherwise noted, is licensed under a Creative Commons Attribution (CC BY) license (<http://creativecommons.org/licenses/by/4.0/>). <https://doi.org/10.1063/5.0107935>

I. INTRODUCTION

Classical molecular dynamics (MD) simulations are a powerful tool to investigate molecular systems *in silico*, providing complementary insights to experiments. Within the discipline of computational chemistry, free-energy calculations are an important (albeit challenging) task, which is nowadays a routine part of computer-aided drug design workflows.^{1–9} Thermodynamic integration (TI),¹⁰ free-energy perturbation (FEP),¹¹ Bennett's acceptance ratio (BAR),¹² and multistate BAR (MBAR)¹³ are examples of well-established pathway-dependent pairwise free-energy methods. In recent years, multistate free-energy methods, such as multi-site λ -dynamics^{14–16} and enveloping distribution sampling (EDS),^{17,18} have emerged, enabling the calculation of pairwise

free-energy differences for multiple end-states from a single simulation. While λ -dynamics is also a pathway-dependent method, no pathway is specified in EDS, which offers additional flexibility for sampling. Replica-exchange EDS (RE-EDS)^{19–22} and accelerated EDS (A-EDS)^{23,24} are extensions of EDS that aim at increasing the accuracy and robustness of the obtained free-energy differences. Currently, both RE-EDS and A-EDS are implemented in the GROMOS MD engine.²⁵

In EDS,^{17,18} N end-states are combined into a reference-state potential V_R as¹⁷

$$V_R(\mathbf{r}; s, \mathbf{E}^R) = -\frac{1}{\beta s} \ln \left[\sum_{i=1}^N e^{-\beta s(V_i(\mathbf{r}) - E_i^R)} \right], \quad (1)$$

where V_i is the total potential energy of end-state i (including solute–solute, solute–environment, and environment–environment components), $s > 0$ is the smoothness parameter, \mathbf{E}^R is a vector of energy offsets, and $\beta = 1/(k_B T)$, where k_B is the Boltzmann constant and T the absolute temperature. While the parameter s smooths the potential-energy landscape and consequently decreases energy barriers, the energy offsets govern the contributions of the individual end-states to the reference-state potential. If the nonbonded interactions are rigorously pairwise separable, the interactions between the unperturbed particles in the system have to be calculated only once for V_R (i.e., not for each end-state), as these terms can be separated out from the sum over the end-states i in Eq. (1), leading to the inherent efficiency of EDS. This typically applies to the covalent interactions as well as the nonbonded environment–environment interactions when using a pairwise interaction scheme.

The force resulting from the reference-state potential on a particle k can be calculated by applying the chain rule as^{17,18}

$$\begin{aligned} \mathbf{f}_k(t) &= -\frac{\partial V_R(\mathbf{r}; s, \mathbf{E}^R)}{\partial \mathbf{r}_k} \\ &= \sum_{i=1}^N \left[\frac{e^{-\beta s(V_i(\mathbf{r}) - E_i^R)}}{\sum_{j=1}^N e^{-\beta s(V_j(\mathbf{r}) - E_j^R)}} \left(-\frac{\partial V_i(\mathbf{r})}{\partial \mathbf{r}_k} \right) \right] \\ &= \sum_{i=1}^N \left[f_i^{\text{scal}} \left(-\frac{\partial V_i(\mathbf{r})}{\partial \mathbf{r}_k} \right) \right], \end{aligned} \quad (2)$$

i.e., the force contribution of each end-state potential V_i is scaled by the scaling factor

$$f_i^{\text{scal}} = \frac{e^{-\beta s(V_i(\mathbf{r}) - E_i^R)}}{\sum_{j=1}^N e^{-\beta s(V_j(\mathbf{r}) - E_j^R)}} = \frac{e^{-\beta s(V_i(\mathbf{r}) - E_i^R)}}{e^{-\beta s V_R(\mathbf{r}; s, \mathbf{E}^R)}}. \quad (3)$$

Note that by definition, it holds that $\sum_{i=1}^N f_i^{\text{scal}} = 1$.

From a single EDS simulation, the free-energy difference between any end-state pair in the system can be calculated as^{17,18}

$$\Delta G^{ji} = G^j - G^i = -\frac{1}{\beta} \ln \frac{\langle e^{-\beta(V_j - V_R)} \rangle_R}{\langle e^{-\beta(V_i - V_R)} \rangle_R}. \quad (4)$$

In practice, the accuracy of free-energy differences obtained from EDS simulations rely critically on the choice of the s -value and of the energy offsets.²⁶ To mitigate the choice of optimal parameters, EDS was combined with Hamiltonian replica exchange (RE)^{27,28} to enhance sampling by simulating multiple EDS replicas with decreasing s -values (but constant \mathbf{E}^R) and by attempting replica exchanges at fixed intervals,¹⁹ following an idea introduced by Brooks and co-workers for constant pH simulations.²⁹ To decide whether the s -values of two replicas k and l with s -values s_i and s_j should be exchanged, a Metropolis–Hastings³⁰ criterion is employed. The probability of an exchange is determined as^{19,28}

$$P_{k,l} = \begin{cases} 1, & \Delta \leq 0, \\ e^{-\beta \Delta}, & \Delta > 0, \end{cases} \quad (5)$$

with $\Delta = (V_R(\mathbf{r}_k; s_j) + V_R(\mathbf{r}_l; s_i)) - (V_R(\mathbf{r}_k; s_i) + V_R(\mathbf{r}_l; s_j))$, where \mathbf{r}_k and \mathbf{r}_l are the current coordinates of replicas k and l , respectively. In recent studies, RE-EDS has been applied to calculate relative binding and hydration free energies for (i) molecules containing relatively large structural changes, such as R-group modifications, ring opening/closing, and ring size changes, and (ii) systems containing a large number of end-states.^{21,22,31}

The calculation of the (pairwise) nonbonded interactions is usually the most expensive part of an MD simulation due to the large number [in principle $\mathcal{O}(N^2)$ for N particles] of particle pairs (depending on the functional form, potentially also triplets, etc.). To improve the computational efficiency, in practice, the nonbonded interactions are only calculated explicitly within a given cutoff distance. The interactions beyond the cutoff are either neglected completely, resulting in a truncation of the nonbonded potential energy, or approximated using a (mean-field or periodic) long-range correction. While a straight truncation is less problematic for van der Waals interactions,³² it can lead to serious cutoff artifacts for electrostatic interactions.^{33–37} Typically, the long-range electrostatic interactions are, therefore, approximated by employing either a reaction-field (RF) correction³⁸ or a lattice-sum scheme, such as Ewald summation,³⁹ particle–particle particle–mesh (P3M),⁴⁰ or particle–mesh Ewald (PME).^{41,42} Recently, Kubincová *et al.* proposed a shifted RF correction that avoids the occurrence of artifacts at the cutoff.⁴³ In the context of RE-EDS simulations, using an RF correction is particularly convenient, as the nonbonded potential-energy contribution of the different end-states can easily be separated. Such a partitioning is required to calculate the reference-state potential V_R [Eq. (1)] efficiently. For lattice-sum schemes, on the other hand, additional fast Fourier transformations (FFTs)⁴⁴ would be required to achieve a partitioning of the end-state energies.⁴⁵

In the present study, we investigate the use of the shifted RF scheme by Kubincová *et al.*⁴³ in RE-EDS simulations, such that the sampling efficiency of RE-EDS is retained while enabling a rigorously conservative treatment of force fields with QM-derived charges (without the need of charge redistributions to achieve neutral charge groups) and facilitating the implementation of RE-EDS in MD software packages other than GROMOS. For this, different choices for the treatment of the electrostatic energy (i.e., functional form, cutoff distance, atom-based or charge-group-based cutoff) are first compared in the context of solvation free-energy calculations with RE-EDS in the GROMOS MD engine.²⁵ Solvation free energies in water and in chloroform are used as a straightforward (and computationally cost-effective) test system to compare methods^{46,47} and implementations. Second, a proof-of-concept implementation of RE-EDS in OpenMM^{48,49} is presented and tested using the shifted RF scheme of Kubincová *et al.*⁴³ The results are compared to the experimental and calculated values reported in the FreeSolv^{50,51} and Minnesota solvation⁵² databases.

II. THEORY

A. Reaction-field correction for long-range electrostatics

In the GROMOS MD engine,^{25,53} long-range electrostatic interactions are usually handled by employing a reaction-field (RF) correction,³⁸

$$V^{\text{ele}} = \sum_i \sum_{j \in \text{PL}(i)} \frac{q_i q_j}{4\pi\epsilon_0 \epsilon_{\text{cs}}} \left[\frac{1}{r_{ij}} - \frac{C_{\text{RF}} r_{ij}^2}{2R_{\text{RF}}^3} - \frac{1 - 0.5C_{\text{RF}}}{R_{\text{RF}}} \right], \quad (6)$$

where q_i and q_j are the charges of atoms i and j , respectively, ϵ_0 is the permittivity of vacuum, ϵ_{cs} is the background dielectric permittivity, r_{ij} is the (minimum-image) distance between atoms i and j , and R_{RF} is the cutoff distance for the pairlist construction.⁵⁴ The notation $j \in \text{PL}(i)$ indicates an atom j with $j > i$, where j is in the pairlist of i . The constant C_{RF} characterizes the effect of the RF continuum as^{38,54}

$$C_{\text{RF}} = \frac{(2\epsilon_{\text{cs}} - 2\epsilon_{\text{RF}})(1 + \kappa_{\text{RF}} R_{\text{RF}}) - \epsilon_{\text{RF}}(\kappa_{\text{RF}} R_{\text{RF}})^2}{(\epsilon_{\text{cs}} + 2\epsilon_{\text{RF}})(1 + \kappa_{\text{RF}} R_{\text{RF}}) + \epsilon_{\text{RF}}(\kappa_{\text{RF}} R_{\text{RF}})^2}, \quad (7)$$

where ϵ_{RF} is the RF dielectric permittivity and κ_{RF} is the inverse Debye screening length.⁵⁵ In simulations with explicit solvent, ϵ_{cs} is usually set to one and κ_{RF} is set to zero.⁵⁵ In this case, the electrostatic potential energy can be calculated as

$$V^{\text{ele}} = \sum_i \sum_{j \in \text{PL}(i)} \frac{q_i q_j}{4\pi\epsilon_0} \left[\frac{1}{r_{ij}} + A_{\text{RF}} r_{ij}^2 - B_{\text{RF}} \right], \quad (8)$$

where the parameters A_{RF} and B_{RF} are calculated as

$$A_{\text{RF}} = \frac{\epsilon_{\text{RF}} - 1}{1 + 2\epsilon_{\text{RF}}} \frac{1}{R_{\text{RF}}^3} \quad (9)$$

and

$$B_{\text{RF}} = \frac{1}{R_{\text{RF}}} + A_{\text{RF}} R_{\text{RF}}^2 = \frac{3\epsilon_{\text{RF}}}{1 + 2\epsilon_{\text{RF}}} \frac{1}{R_{\text{RF}}}. \quad (10)$$

In the GROMOS MD engine, there is additionally an RF contribution for excluded neighbors as well as a self-interaction. The self-interaction may be interpreted as the reversible work needed to individually charge the atoms at infinite separation.⁵⁶ Thus, the total electrostatic potential energy is calculated as^{57–59}

$$V^{\text{ele, orig}} = \sum_i \sum_{j \in \text{PL}(i)} \frac{q_i q_j}{4\pi\epsilon_0} \left[\frac{\alpha_{ij}}{r_{ij}} + A_{\text{RF}} r_{ij}^2 - B_{\text{RF}} \right] - \frac{1}{2} \frac{B_{\text{RF}}}{4\pi\epsilon_0} \left[\sum_i q_i^2 - \frac{1}{\epsilon_{\text{RF}}} \left(\sum_i q_i \right)^2 \right], \quad (11)$$

where α_{ij} is set to zero if atoms i and j are excluded neighbors and to one otherwise. Note that the sum over all charges, $\sum_i q_i$, is zero for neutral systems and the corresponding term $\epsilon_{\text{RF}}^{-1} (\sum_i q_i)^2$ is currently not implemented in GROMOS. When using AMBER/GAFF topologies⁶⁰ in GROMOS,²² the scaling of the electrostatic 1,4-interactions by a factor 1/1.2^{60,61} is accounted for by setting α_{ij} to 1/1.2 if atoms i and j are third neighbors. It should be noted that the choice of B_{RF} in Eq. (10) only leads to an interaction energy that is continuous at R_{RF} for normal pairs, i.e., those for which $\alpha_{ij} = 1$. Although continuity could be enforced also for the pairs with $\alpha_{ij} \neq 1$ by adjusting B_{RF} for these pairs, this choice is not made here for two reasons: (i) Excluded and third-neighbor pairs correspond to close covalent neighbors, so that they are and stay within the cutoff throughout a simulation; and (ii) close-neighbor modifications are meant to reduce the direct Coulombic interactions

between the atoms without altering their effective interactions via the environment. Furthermore, note that the B_{RF} term does not have an inherent physical meaning. It merely ensures that the electrostatic potential is continuous (and thus differentiable) at the cutoff R_{RF} . A “physical alternative” to $V^{\text{ele, orig}}$ is, therefore,

$$V^{\text{ele, phys}} = \sum_i \sum_{j \in \text{PL}(i)} \frac{q_i q_j}{4\pi\epsilon_0} \left[\frac{\alpha_{ij}}{r_{ij}} + A_{\text{RF}} r_{ij}^2 \right]. \quad (12)$$

For computational efficiency and to avoid cutoff noise when employing a straight-cutoff scheme, multiple atoms of a molecule can be grouped into “charge groups” (CGs) with integer total charges.⁶² In the GROMOS MD engine, the position of a solute CG is calculated as its center of geometry (COG), whereas the position of a solvent CG is set to the position of the first atom of the solvent molecule (e.g., the oxygen atom for water).⁵⁵ When employing a CG-based cutoff, the pairlist algorithm takes the CG positions into account instead of the individual atom coordinates to determine whether two atoms are currently within the cutoff (Fig. 1, right). GROMOS (compatible) force fields typically make use of CGs,^{54,63–67} whereas most other force-field families use an atom (AT)-based cutoff (Fig. 1, left).⁵⁴ There are several reasons to prefer AT truncation for force-field development. In practice, it is difficult to automate the generation of neutral charge groups within molecules.⁶⁸ Furthermore, CG truncation can result in a loss of energy conservation and heating^{69,70} and lead to other artifacts.^{36,71–73}

CG cutoff is implemented, e.g., in the GROMOS²⁵ and GROMACS⁷⁴ MD engines (though its use is deprecated in the latter since GROMACS 5.0⁷⁵). In the AMBER⁷⁶ and OpenMM⁴⁹ MD engines, on the other hand, only AT cutoff is implemented. As the AMBER force fields use QM-derived partial charges, no CGs are defined. In our previous study on converting AMBER topologies with the *amber2gromos* program for RE-EDS

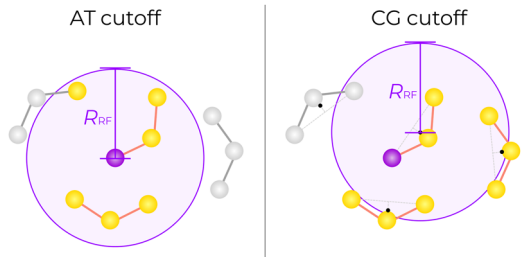


FIG. 1. Schematic illustration of atom (AT)-based and charge-group (CG)-based cutoff for nonbonded interactions. The currently considered atom is colored in purple, and the atoms in its pairlist are colored in yellow, whereas the atoms outside the pairlist are colored in gray. Here, the CGs are defined such that they each contain all three atoms of the depicted molecules. Note that the configurations and currently considered atom are identical on the left and on the right. (Left) For AT cutoff, all atoms within R_{RF} of the current atom are considered for the nonbonded interactions. (Right) For CG cutoff, all atoms belonging to CGs whose center of geometry (COG, black dot) is within R_{RF} of the COG of the current atom's CG are considered for the nonbonded interactions. Note that instead of the COG, sometimes the first atom of the CG is used as the reference point (e.g., for solvent molecules in GROMOS).⁵⁵

simulations using the GROMOS MD engine,²² the solute molecules were small enough that a single CG per molecule could be justified. For larger molecules, however, this is no longer appropriate. To address this issue, we want to bypass CGs altogether by employing an AT cutoff in the RE-EDS simulations. This is achieved using the RF scheme with a shifting function developed by Kubincová *et al.*⁴³ The scheme significantly reduces cutoff artifacts, i.e., cutoff noise in the radial distribution functions and dipole–dipole orientation correlation functions of several model liquids.

B. Reaction-field scheme for atom-based cutoff

In the RF scheme with a shifting function, the electrostatic potential energy is defined as⁴³

$$V^{\text{ele, shift}} = \sum_i \sum_{j \in \text{PL}(i)} \frac{q_i q_j}{4\pi\epsilon_0} \left[\frac{\alpha_{ij}}{r_{ij}} + A_{\text{RF}} r_{ij}^2 + a_{\text{RF},4} r_{ij}^4 + a_{\text{RF},6} r_{ij}^6 - B_{\text{RF}}^{\text{shift}} \right] - \frac{1}{2} \frac{B_{\text{RF}}^{\text{shift}}}{4\pi\epsilon_0} \left[\sum_i q_i^2 - \frac{1}{\epsilon_{\text{RF}}} \left(\sum_i q_i \right)^2 \right], \quad (13)$$

where $a_{\text{RF},4}$ and $a_{\text{RF},6}$ are shifting parameters chosen such that the potential-energy function is not modified in the limit $r_{ij} \rightarrow 0$, is continuous at the cutoff, and is constant at and beyond the cutoff; the exerted force (i.e., first derivative) resulting from it is zero at the cutoff; and the force derivative itself (i.e., second derivative) is also zero at the cutoff.⁴³ Furthermore, $B_{\text{RF}}^{\text{shift}}$ is defined as

$$B_{\text{RF}}^{\text{shift}} = B_{\text{RF}} + a_{\text{RF},4} R_{\text{RF}}^4 + a_{\text{RF},6} R_{\text{RF}}^6. \quad (14)$$

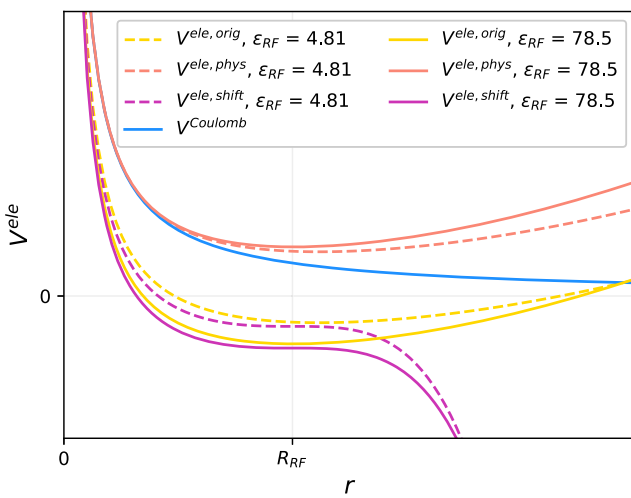


FIG. 2. Schematic illustration of different functional forms of V^{ele} . Three different functional forms of V^{ele} are shown for the electrostatic interaction between two model particles ($q_0, q_1 > 0$), viz., $V^{\text{ele, orig}}$ [Eq. (11), yellow], $V^{\text{ele, phys}}$ [Eq. (12), orange], and $V^{\text{ele, shift}}$ [Eq. (13), purple], for two different RF permittivities, viz., $\epsilon_{\text{RF}} = 4.81$ (chloroform, dashed lines) and $\epsilon_{\text{RF}} = 78.5$ (water, solid lines).^{58,77} Additionally, $V_{0,1}^{\text{Coulomb}} = q_0 q_1 / (4\pi\epsilon_0 r_{0,1})$ is depicted in blue. (Left) The potential-energy functions are shown for a nonperiodic system without cutoff truncation (note that the use of RF without a spherical cutoff represents a hypothetical scenario and is not used in practice). (Right) The potential-energy functions are shown with the cutoff R_{RF} in a periodic box with box length a .

Note that in the modified GROMOS implementation used in the current study, $V^{\text{ele, shift}}$ is calculated via the equivalent equation⁴³

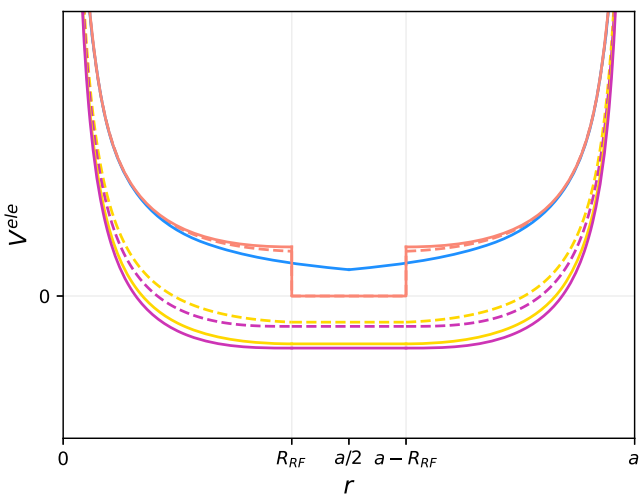
$$V^{\text{ele, shift}} = \sum_i \sum_{j \in \text{PL}(i)} \frac{q_i q_j}{4\pi\epsilon_0} \left[\frac{\alpha_{ij}}{r_{ij}} + A_{\text{RF}} r_{ij}^2 + a_{\text{RF},4} r_{ij}^4 + a_{\text{RF},6} r_{ij}^6 \right] + \sum_i \sum_{j \notin \text{PL}(i)} \frac{q_i q_j}{4\pi\epsilon_0} B_{\text{RF}}^{\text{shift}}. \quad (15)$$

The second term of Eq. (15) (i.e., the sum over the atom pairs outside the pairlist) can be calculated as⁴³

$$\sum_i \sum_{j \notin \text{PL}(i)} \frac{q_i q_j}{4\pi\epsilon_0} B_{\text{RF}}^{\text{shift}} = \frac{B_{\text{RF}}^{\text{shift}}}{4\pi\epsilon_0} \left[\sum_i \sum_{j > i} q_i q_j - \sum_i \sum_{j \in \text{PL}(i)} q_i q_j \right]. \quad (16)$$

Note that in Eq. (16), the prefactor $B_{\text{RF}}^{\text{shift}}/(4\pi\epsilon_0)$ and the first term in the brackets are configuration independent, i.e., they need to be calculated only once at the start of the simulation and do not induce any atomic force.⁴³ It can be shown that for neutral systems [i.e., $(\sum_i q_i)^2 = 0$], Eqs. (13) and (15) are equivalent. In the near future, the modified GROMOS implementation will be adapted to use Eq. (13) instead as this formulation is more similar to the implementation of the native GROMOS RF and will require fewer modifications to the outer and inner nonbonded loops. The corresponding code will be included in the next release of GROMOS. An illustration of the three presented functional forms of V^{ele} is provided in Fig. 2.

The modified electrostatic energy term $V^{\text{ele, shift}}$ can easily be “corrected” to $V^{\text{ele, orig}}$ [Eq. (11)] or $V^{\text{ele, phys}}$ [Eq. (12)] for a given energy trajectory by keeping track of the extra energy (i.e., the difference between $V^{\text{ele, shift}}$ and $V^{\text{ele, orig}}$ or $V^{\text{ele, phys}}$, respectively) during the simulation. For a RE-EDS simulation in which $V^{\text{ele, shift}}$ was used



to propagate the system, the corrected end-state energy for end-state i can then be calculated as

$$V_i^{\text{shift} \rightarrow \text{orig}} = V_i + V_i^{\text{extra, orig}}, \quad (17)$$

$$V_i^{\text{shift} \rightarrow \text{phys}} = V_i + V_i^{\text{extra, phys}}. \quad (18)$$

The corrected reference-state energy can then be calculated as

$$V_R^{\text{shift} \rightarrow \text{orig}} = -\frac{1}{\beta s} \ln \left[\sum_{i=1}^N e^{-\beta s(V_i + V_i^{\text{extra, orig}} - E_i^R)} \right], \quad (19)$$

$$V_R^{\text{shift} \rightarrow \text{phys}} = -\frac{1}{\beta s} \ln \left[\sum_{i=1}^N e^{-\beta s(V_i + V_i^{\text{extra, phys}} - E_i^R)} \right]. \quad (20)$$

This allows us to propagate the system based on the modified electrostatic potential $V^{\text{ele, shift}}$, avoiding artifacts at the cutoff, but calculate the Hamiltonian and free-energy differences based on the energies obtained with the “original” GROMOS electrostatic energies or the “physical” electrostatic energies. The former option potentially achieves more accurate results when using force fields that were parameterized with $V^{\text{ele, orig}}$ (i.e., most GROMOS or GROMOS-compatible force fields), while the latter option might provide more accurate short-range interaction energies.

The modified functional form of V^{ele} (i.e., $V^{\text{ele, shift}}$) allows for the use of an RF correction with an AT cutoff while avoiding artifacts at the cutoff. As the partitioning of the end-state energies is trivial with such an RF correction, it can conveniently be combined with RE-EDS. This is a key advantage for porting the RE-EDS free-energy method to MD engines that do not support the use of CG cutoff. Note that the application of the shifted RF correction to non-neutral systems is in principle possible, but it might require additional correction terms^{78–80} in practice and has to be validated.

III. METHODS

A. Comparison of functional forms of the electrostatic potential energy

To assess whether RE-EDS calculations in GROMOS achieve accurate free-energy estimates with an AT cutoff, free-energy differences in vacuum ($\Delta G_{\text{vac}}^{ji}$), water ($\Delta G_{\text{wat}}^{ji}$), and chloroform ($\Delta G_{\text{CHCl}_3}^{ji}$) were calculated with RE-EDS for two sets of molecules (see Sec. III D). The corresponding relative hydration free energies ($\Delta \Delta G_{\text{hyd}}^{ji} = \Delta G_{\text{wat}}^{ji} - \Delta G_{\text{vac}}^{ji}$) and relative solvation free energies in chloroform ($\Delta \Delta G_{\text{CHCl}_3}^{ji} = \Delta G_{\text{CHCl}_3}^{ji} - \Delta G_{\text{vac}}^{ji}$) were calculated and subsequently compared to experimental and calculated reference values ($\Delta \Delta G_{\text{hyd}}^{ji} = \Delta G_{\text{hyd}}^j - \Delta G_{\text{hyd}}^i$ and $\Delta \Delta G_{\text{CHCl}_3}^{ji} = \Delta G_{\text{CHCl}_3}^j - \Delta G_{\text{CHCl}_3}^i$, respectively).

Three schemes to calculate V^{ele} were compared: (i) $V^{\text{ele, orig}}$ with CG cutoff, (ii) $V^{\text{ele, orig}}$ with AT cutoff, and (iii) $V^{\text{ele, shift}}$ with AT cutoff. In the following, the combination of $V^{\text{ele, orig}}$ with a CG cutoff will be referred to as CG^{orig}, $V^{\text{ele, orig}}$ with an AT cutoff will be referred to as AT^{orig}, and $V^{\text{ele, shift}}$ with an AT cutoff will be referred to as AT^{shift}. Additionally, for the simulations performed using AT^{shift}, we investigated whether using the corrected end-state and reference-state potential energies $V^{\text{shift} \rightarrow \text{orig}}$

and $V^{\text{shift} \rightarrow \text{phys}}$ [Eqs. (17)–(20)] would improve the accuracy of free-energy calculations with RE-EDS.

B. RE-EDS implementation in OpenMM

We developed a proof-of-concept implementation of RE-EDS using the OpenMM MD engine. It consists of a simple Python3 module that relies on the *openmm*,⁴⁹ *parmed*,⁸¹ *numpy*,⁸² and *pandas*⁸³ modules. The source code is available at [https://github.com/rinikerlab/reeds/blob/openmm/reeds_openmm.py](https://github.com/rinikerlab/reeds/blob/openmm/reeds/openmm/reeds_openmm.py) with example scripts provided at <https://github.com/rinikerlab/reeds/tree/main/examples/openmm>.

1. Calculation of the electrostatic potential energy

For RE-EDS to be efficient, the separation of the nonbonded potential-energy contributions from the solute–solute, solute–environment, and environment–environment interactions is essential. While it is trivial for the van der Waals interactions, we decided to use $V^{\text{ele, shift}}$ [Eq. (13)] for the electrostatic interactions.

OpenMM provides the possibility to create so-called *custom forces*.⁴⁹ A custom force is defined by an algebraic expression representing an interaction between particles (or between a particle and an external force), i.e., a potential-energy term, which is then analytically differentiated by OpenMM to obtain the resulting force.⁴⁹ In our module, the nonbonded interactions (including the shifted RF) are implemented via four *CustomNonbondedForce* and *CustomBondForce* terms for each end-state. The per particle and per bond parameters required to characterize the custom forces are taken from the default *NonbondedForce* of the system. Note that the parameters are loaded via *parmed*,⁸¹ allowing the conversion of different topology formats to a format compatible with OpenMM. Upon creation of the custom forces, the default *NonbondedForce* is removed from the system and replaced by the custom forces. For each EDS end-state, a separate force group is defined containing the four custom forces of that end-state, allowing for the separate evaluation of the nonbonded potential energies of the different end-states.

First, for each end-state k , a *CustomNonbondedForce* term is created as

$$V_{k,ij}^{\text{LJ,CRF}} = 4\epsilon_{ij} \left[\left(\frac{\sigma_{ij}}{r_{ij}} \right)^{12} - \left(\frac{\sigma_{ij}}{r_{ij}} \right)^6 \right] + \frac{q_i q_j}{4\pi\epsilon_0} \times \left(\frac{1}{r_{ij}} + A_{\text{RF}} r_{ij}^2 + a_{\text{RF},4} r_{ij}^4 + a_{\text{RF},6} r_{ij}^6 - B_{\text{RF}}^{\text{shift}} \right), \quad (21)$$

to account for the nonbonded interactions of particles i and j that are neither third-neighbor nor excluded pairs. For each end-state, the interaction groups are defined such that the particles of the current end-state interact with the other particles of the current end-state as well as with the environment particles. Note that the particles of an end-state do not include any dummy particles (i.e., the number of particles in end-state i is not necessarily the same as the number of particles in end-state j), which is different from the GROMOS implementation. In addition to the force groups for the end-states, there is one instance of $V_{\text{env},ij}^{\text{LJ,CRF}}$ [analogous to Eq. (21)] that accounts for the intramolecular and intermolecular interactions of the environment particles.

Next, for each end-state k (plus the environment), a *CustomBondForce* term is created as

$$V_{k,ij}^{\text{LJ,CRF},1-4} = 4\epsilon_{ij} \left[\left(\frac{\sigma_{ij}}{r_{ij}} \right)^{12} - \left(\frac{\sigma_{ij}}{r_{ij}} \right)^6 \right] + \frac{q_{ij}^{\text{scal}}}{4\pi\epsilon_0} \frac{1}{r_{ij}} + \frac{q_{ij}}{4\pi\epsilon_0} \times \left(A_{\text{RF}} r_{ij}^2 + a_{\text{RF},4} r_{ij}^4 + a_{\text{RF},6} r_{ij}^6 - B_{\text{RF}}^{\text{shift}} \right), \quad (22)$$

to account for the third-neighbor interactions. Here, a “bond” is added for each third-neighbor pair of the current end-state molecule (or the environment molecules). The parameter q_{ij}^{scal} corresponds to the scaled charge product of the excluded atom pair according to the default *NonbondedForce*, whereas $q_{ij} = q_i q_j$ is the unscaled charge product calculated from the particle charges.

Next, another *CustomBondForce* term is defined as

$$V_{k,ij}^{\text{CRF,excl}} = \frac{q_{ij}}{4\pi\epsilon_0} \left(A_{\text{RF}} r_{ij}^2 + a_{\text{RF},4} r_{ij}^4 + a_{\text{RF},6} r_{ij}^6 - B_{\text{RF}}^{\text{shift}} \right), \quad (23)$$

for each end-state k (plus the environment) to account for the RF contribution of the excluded atom pairs. Here, a “bond” is added for each pair of excluded atoms of the current end-state molecule (or the environment molecules).

Finally, for each end-state k (plus the environment), a *CustomBondForce* term is defined as

$$V_{k,ii}^{\text{self}} = -\frac{1}{2} \frac{B_{\text{RF}}^{\text{shift}}}{4\pi\epsilon_0} q_{ii}, \quad (24)$$

to account for the self-term. Here, a “bond” is added for each atom with itself, and the parameter q_{ii} is calculated as $q_{ii} = q_i q_i$. Note that, analogous to the GROMOS implementation, the term $\epsilon_{\text{RF}}^{-1} (\sum_i q_i)^2$ of Eq. (13) (which is zero for a neutral system) is currently not implemented for simplicity but can easily be added.

2. EDS integration

To perform an integration step of an EDS simulation, the nonbonded forces of the end-states have to be scaled according to Eq. (2). This is achieved in OpenMM via a four-step process: (i) Calculate the nonbonded potential energies of all end-states [Eqs. (21)–(24)]; (ii) calculate the scaling factor f_i^{scal} [Eq. (3)] for each end-state i based on the end-state potential energies calculated in step (i); (iii) scale the nonbonded force resulting from each end-state i by the corresponding scaling factor f_i^{scal} ; and (iv) perform an OpenMM simulation step. For the scaling of the nonbonded forces, the nonbonded potential-energy terms [Eqs. (21)–(24)] of each end-state i are multiplied by the scaling factor f_i^{scal} obtained in step (ii). Note that this integration scheme results in the custom forces of each end-state being evaluated twice per integration step: (i) to calculate the energies and scaling factors and (ii) to calculate the forces. This introduces an inefficiency and will be improved in a future implementation by using a *CustomIntegrator*.

3. Atom-atom distance restraints

When using a dual-topology approach,^{84,85} the coordinates of all molecules are explicitly present during a (RE-)EDS simulation.³¹ To prevent the molecules from drifting apart during the simulation, atom-atom distance restraints can be employed.^{26,31} Here, the distance restraint for a restrained atom pair i and j was added as a *CustomBondForce* with the harmonic potential

$$V_{ij}^{\text{restr}} = \frac{1}{2} K r_{ij}^2, \quad (25)$$

where K is the force constant of the distance restraint. Details on how the atom-atom distance restraints were generated for the simulations are provided in Sec. III E.

4. RE-EDS simulation

Sections III B 1–III B 3 describe the three ingredients needed to implement an EDS simulation with OpenMM: separable nonbonded energy terms, an integration procedure, and atom-atom distance restraints. For a RE-EDS simulation, two more ingredients are needed: (i) EDS simulations of independent replicas at different s -values at the same time and (ii) replica exchanges. In the current “proof-of-concept” implementation, the replicas are propagated serially on the GPU, i.e., n EDS integration steps are performed for the first replica (where n is the number of time steps between exchanges), then n steps are performed for the next replica, etc. This is, of course, inefficient and will be parallelized in a future implementation. After the n steps have been performed for each replica, replica exchanges are attempted. When comparing two neighboring replicas, the exchange probability is calculated according to Eq. (5).

C. RE-EDS pipeline

To perform RE-EDS simulations in GROMOS, the pipeline recently proposed by Ries *et al.*²¹ was used. The RE-EDS pipeline is carried out using the Python³⁸⁶ *reeds* module freely available on Github at <https://github.com/rinikerlab/reeds>.⁸⁷ It consists of three main steps: parameter exploration, parameter optimization, and production. During the parameter exploration step, relevant configurations are generated for all end-states, a lower bound is determined for the s -values, and initial estimates for the energy offsets are generated. Next, during parameter optimization, the distribution of the s -values and the values of the energy offsets E^R are optimized such that frequent round trips are observed for all replicas, and all end-states are sampled approximately equally at $s = 1$. Finally, the free-energy differences between all end-state pairs are calculated from a RE-EDS production run with the optimized parameters. To perform the RE-EDS calculations in OpenMM, a slightly modified version of the *reeds* module was used.

D. Datasets

In order to (a) assess the performance of the different RF schemes and cutoff values and (b) validate the implementation of RE-EDS in OpenMM, three different sets of molecules were considered. A set of six benzene derivatives (labeled set A) was taken from a previous study.²² Set A consists of six benzene derivatives selected from the FreeSolv^{50,51} database with available experimental

and calculated reference data. In addition, two new sets of molecules (labeled set C and set D, respectively) were assembled. For both sets, the selected molecules were contained in both the FreeSolv and the Minnesota (chloroform) solvation⁵² database, such that experimental reference data were available both for hydration free energies and for solvation free energies in chloroform. This allowed the comparison of the different RF schemes and cutoff values both in a high permittivity (water) and in a low permittivity (chloroform) environment. Set C contains 14 benzene derivatives with small substituents (Fig. 3, top) and is a subset of set B from a previous publication²² (i.e., the molecules of set B for which solvation free energies in chloroform were available from the Minnesota solvation database). Set D consists of 13 benzene, pyridine, and pyrazine derivatives with larger substituents (Fig. 3, bottom).

E. Simulation details

All topologies were generated with *tleap* (AmberTools16)⁶¹ based on the mol2 and frcmod files provided in the FreeSolv database.^{50,51} For the simulations in GROMOS, the topologies were converted with *amber2gromos* and for the simulations in OpenMM, the topologies were converted using *parmed*.⁸¹

The partial charges were generated with antechamber^{60,88} using the AM1-BCC^{89,90} method. The input files for the RE-EDS simulations in GROMOS were prepared using *amber2gromos* as well as the GROMOS++⁹¹ programs *pdb2g96*, *red_top*, and

prep_eds.²² The alignment of the molecules was generated with the RDKit⁹² module *rdFMCS* and the *AllChem.AlignMol* function. The aligned molecule pairs were selected manually to maximize the overlap of the respective aromatic rings and substituents. For some of the molecule pairs, all atom types were matched (*rdFMCS.AtomCompare.CompareAny*), whereas for others, only heavy atom types were matched (*rdFMCS.AtomCompare.CompareAnyHeavyAtom*).²² To prevent the molecules from drifting apart from each other during the RE-EDS simulations, atom–atom distance restraints were employed. They were generated with *RestraintMaker*.³¹ For multistate simulations, the program *RestraintMaker* generates (locally) optimal atom–atom distance restraints between pairs of molecules based on a greedy algorithm, resulting in a cycle of pairwise restrained molecules.³¹ Here, four atom–atom distance restraints were generated per molecule pair. The same atom pairs were restrained for the simulations in GROMOS and in OpenMM.

The RE-EDS simulations in GROMOS were performed with a modified version of GROMOS^{25,93} 1.5.0. The RE-EDS pipeline was carried out using the open-source *reeds* module.⁸⁷ The RE-EDS simulations in OpenMM were performed with OpenMM version 7.7.0⁴⁹ and the RE-EDS pipeline was carried out using a slightly modified version of the *reeds* module. The TIP3P⁹⁴ water model was used for the simulations in water. The integration time step was set to 2 fs. The RF permittivity ϵ_{RF} was set to 1 in vacuum, 4.81 in chloroform,⁹⁵ and 78.5 in water.^{58,77,96} For the simulations

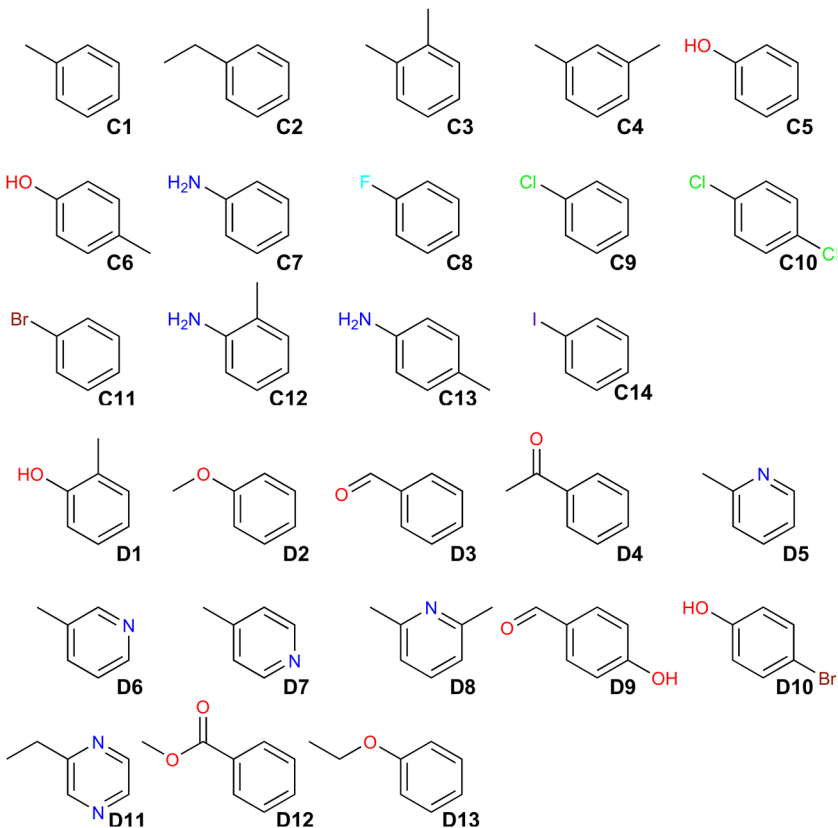


FIG. 3. (Top) Set C consists of 14 benzene derivatives, selected from the FreeSolv^{50,51} and the Minnesota (chloroform) solvation⁵² database. A list of the corresponding molecule indices, the FreeSolv identifiers, the Minnesota solvation database identifiers, the simplified molecular input line-entry system (SMILES) strings, and the names of the molecules can be found in Table S1 in the *supplementary material*. (Bottom) Set D consists of 13 benzene, pyridine, and pyrazine derivatives, selected from the FreeSolv^{50,51} and the Minnesota (chloroform) solvation⁵² database. A list of the corresponding molecule indices, the FreeSolv identifiers, the Minnesota solvation database identifiers, the SMILES strings, and the names of the molecules can be found in Table S2 in the *supplementary material*.

in GROMOS, three different choices of R_{RF} (i.e., 0.8, 1.0, and 1.2 nm) were compared. For the simulations in OpenMM, R_{RF} was set to 1.2 nm. The temperature was maintained at 298.15 K in all environments and the pressure at 0.061 02 kJ mol⁻¹ nm⁻³ ≈ 1.013 25 bar ≈ 1 atm in chloroform/water. In GROMOS, Berendsen thermostat and barostat⁹⁷ were employed for the simulations in water and chloroform. In vacuum, the leap-frog stochastic dynamics integrator was used such that no temperature scaling was necessary. In OpenMM, a Monte Carlo barostat⁹⁸ was employed for the simulations in chloroform/water. For the OpenMM simulations in all environments, the *LangevinMiddleIntegrator* was used; thus, no additional temperature scaling was necessary. All bonds were constrained with the SHAKE algorithm⁹⁹ in GROMOS (relative tolerance of 10⁻⁴), or with a mix of SETTLE,¹⁰⁰ SHAKE,⁹⁹ and CCMA¹⁰¹ in OpenMM (i.e., default). The force constant for the atom–atom distance restraints was set to³¹ 5000 kJ mol⁻¹ nm⁻². All simulations were executed on the Euler cluster of ETH Zürich. The input files for the RE-EDS simulations can be found at https://github.com/rinikerlab/reeds/tree/main/examples/systemsshifted_reaction_field.

The calculated hydration free energies reported in the FreeSolv^{50,51} database were obtained from alchemical MBAR^{12,13,102} simulations performed with the GROMACS MD engine.^{74,103} 20 λ -values were used and the simulations at each λ -value were 5 ns long. The electrostatic interactions were modified along the first 5 intermediate states and the Lennard-Jones interactions were modified along the last 15 intermediate states.⁵¹

1. Set A

For the RE-EDS simulations in GROMOS/OpenMM, six independent EDS simulations of 1 ns length with $s = 1$ were conducted to generate optimized coordinates for each end-state in vacuum/water. For each EDS simulation, there was one “favored” end-state. The energy offset of the favored end-state was set to 500 kJ mol⁻¹, whereas the energy offset of the other end-states were set to -500 kJ mol⁻¹. 21 independent EDS simulations of 0.2 ns length with logarithmically distributed s -values between 1 and 10⁻⁵ were used to determine a lower bound for the s -values. The determined lower bounds were identical for the GROMOS and OpenMM simulations (0.0178 in vacuum and 0.01 in water). Next, the energy offsets were estimated from a RE-EDS simulation of 0.8 ns length with 11 replicas for vacuum and 12 replicas for water, respectively, where the initial energy offsets were all set to zero. In vacuum, one s -optimization run of 0.5 ns length with 12 replicas was required to obtain frequent round trips in vacuum, adding four s -values. In water, two s -optimization iterations—one of 0.5 ns length with 13 replicas and one of 1.0 ns length with 17 replicas—were required, adding eight s -values in total. In vacuum, no energy offset rebalancing was needed. In water, two energy offset rebalancing runs of 0.5 ns length each with 21 replicas were required to sample all end-states approximately equally. Finally, the production runs were 0.5 ns in vacuum (11 replicas) and in water (16 replicas). The free-energy differences in vacuum/water were calculated from five independent production runs.

2. Set C

For set C, nine independent RE-EDS pipelines were executed in GROMOS for each environment (vacuum/water/chloroform).

Three different schemes to calculate the electrostatic potential energy were used: CG^{orig}, AT^{orig}, and AT^{shift}. Furthermore, three different cutoffs were used for each scheme: 0.8, 1.0, and 1.2 nm. For each RE-EDS pipeline, 14 independent EDS simulations were conducted analogously to set A to generate optimized coordinates for the RE-EDS simulations. The lower bound search was analogous to set A for all systems. The determined lower bounds were between 0.0178 and 0.01. For each RE-EDS pipeline, the energy offsets were estimated from RE-EDS simulations of 1.2 ns. The number of replicas was either 19 (lower bound, 0.0178) or 20 (lower bound, 0.01). In vacuum/chloroform, one s -optimization run of 1 ns length was conducted, adding four s -values. In water, two s -optimization runs of 1 and 1.5 ns, respectively, were performed, adding eight s -values in total. Four energy offset rebalancing runs of 0.5 ns length each were conducted in vacuum, two in chloroform, and three in water. The production runs were 1 ns in vacuum and 2 ns in chloroform/water. The free-energy differences in vacuum/chloroform/water were calculated from five independent production runs each.

For the RE-EDS calculations in OpenMM, only the system with the scheme AT^{shift} and a 1.2 nm cutoff was investigated. The coordinate optimization was analogous to the RE-EDS simulations in GROMOS, as was the lower bound search. The determined lower bounds were identical to the ones obtained from the simulations in GROMOS. For the energy offset estimation, simulations of 0.8 ns length were conducted in each environment with 19 replicas for vacuum and 20 replicas for chloroform/water. In vacuum/chloroform, one s -optimization run of 0.5 ns, adding four s -values, was sufficient, whereas in water, two s -optimization runs of 0.5 ns were used, adding eight s -values in total. In vacuum/water, three energy offset rebalancing runs of 0.5 ns length each were conducted, and in chloroform, two energy offset rebalancing runs of 0.5 ns length each were performed. The production runs were 1 ns in vacuum and 2 ns in chloroform/water. Again, the free-energy differences in vacuum/chloroform/water were calculated from five independent production runs.

3. Set D

For set D, nine independent RE-EDS pipelines were executed in GROMOS in each of the three environments, analogously to set C. The coordinate optimization (13 independent EDS simulations) and lower bound search were analogous to those for set C. The determined lower bounds were between 0.0178 and 0.003 16. The number of replicas for the energy offset estimation was between 18 (lower bound, 0.0178) and 22 (lower bound, 0.003 16). The s -optimization runs were analogous to those for set C. For the simulations in vacuum, three energy offset rebalancing runs of 0.5 ns length each were required, while the energy offset rebalancing runs were identical to those for set C in chloroform/water. The production runs were analogous to those for set C in all three environments and the free-energy differences were again calculated from five independent production runs.

As for set C, only the system with the scheme AT^{shift} and a 1.2 ns cutoff was investigated with OpenMM. Moreover, the coordinate optimization and lower bound search here were analogous to those for the RE-EDS simulations in GROMOS. The lower bounds

were 0.0178 for vacuum and 0.0056 for chloroform/water, identical to the ones obtained in GROMOS. 18 replicas were used for the energy offset estimation in vacuum and 20 replicas for the energy offset estimation in water/chloroform. In vacuum/chloroform, one *s*-optimization run of 0.5 ns length was sufficient, adding four *s*-values, whereas in water, two *s*-optimization runs of 0.5 ns length each were used, adding eight *s*-values in total. In vacuum/chloroform, two energy offset rebalancing runs (0.5 ns each) were required, and in water, three rebalancing runs (0.5 ns each) were required. The production runs were analogous to the simulations in GROMOS and the free-energy differences were calculated from five independent production runs.

F. Analysis

The analysis of the simulations was conducted with GROMOS++⁹¹ and PyGromosTools.¹⁰⁴ Furthermore, the following Python packages were used for visualization and analysis: Matplotlib,¹⁰⁵ mpmath,¹⁰⁶ NumPy,⁸² Pandas,⁸³ SciPy,¹⁰⁷ and Seaborn.¹⁰⁸ For all systems, the root-mean-square error (RMSE), the mean absolute error (MAE), and the Spearman¹⁰⁹ correlation coefficient between the different simulation methods and the experimental values are reported. Note that all Spearman correlation coefficients are reported for the extended set of $\Delta\Delta G$ values with both signs (i.e., $\Delta\Delta G^{ji}$ as well as $\Delta\Delta G^{ij} = -\Delta\Delta G^{ji}$) to provide a robust measure of correlation irrespective of the directions of the free-energy calculations.¹¹⁰ The free-energy differences obtained from the RE-EDS simulations in GROMOS were calculated with the GROMOS++ program *dmult*, whereas the free-energy differences obtained from the RE-EDS simulations in OpenMM were calculated directly with Python using the NumPy functions *log*, *exp*, and *mean*.

IV. RESULTS

A. Comparison of different RF schemes and cutoff values for RE-EDS

The relative hydration free energies, $\Delta\Delta G_{\text{hyd}}$, and the relative solvation free energies in chloroform, $\Delta\Delta G_{\text{CHCl}_3}$, were calculated from the free-energy differences obtained with RE-EDS in GROMOS for sets C and D. The resulting $\Delta\Delta G_{\text{hyd}}$ values were compared to the values obtained from the calculated and experimental ΔG_{hyd} values reported in the FreeSolv database.^{50,51} The $\Delta\Delta G_{\text{CHCl}_3}$ values were compared to the ones obtained from the experimental ΔG_{CHCl_3} values reported in the Minnesota solvation database.⁵²

1. RF schemes and cutoff values

First, the $\Delta\Delta G_{\text{hyd}}$ and $\Delta\Delta G_{\text{CHCl}_3}$ values obtained from the RE-EDS calculations in GROMOS for the different RF schemes (i.e., CG^{orig}, AT^{orig}, AT^{shift}) with different cutoff values (i.e., 0.8, 1.0, 1.2 nm) were evaluated.

a. Set C. For set C, the agreement between the $\Delta\Delta G_{\text{hyd}}$ values obtained from RE-EDS in GROMOS and the calculated/experimental results reported by FreeSolv was high for all schemes. Relative to the experimental values, the RMSE values are between 2.1 and 2.8 kJ mol⁻¹ and the Spearman correlation coefficients between 0.84 and 0.91 (bottom left panel in Fig. 4, Table I).

While the reported metrics are slightly better for CG^{orig} than for the two schemes with AT cutoff, the differences are negligible at $R_{\text{RF}} = 1.2$ nm. The RMSE values compared to MBAR are between 0.4 and 1.1 kJ mol⁻¹ and the Spearman correlation coefficients between 0.96 and 0.99 (bottom middle panel in Fig. 4, Table S3 in the supplementary material).

The agreement between the $\Delta\Delta G_{\text{CHCl}_3}$ values obtained from RE-EDS in GROMOS and the experimental results reported in the Minnesota solvation database⁵² was lower than for the hydration free energies. Apart from one outlier (CG^{orig} with $R_{\text{RF}} = 0.8$), the RMSE values are between 3.3 and 3.7 kJ mol⁻¹ and the Spearman correlation coefficients between 0.59 and 0.85 (bottom right panel in Fig. 4, Table I). The reported metrics improved with an increase in R_{RF} for all three RF schemes.

b. Set D. While the agreement between RE-EDS and MBAR was again excellent, the deviations from the experimental reference data were considerably higher for set D than for set C. This indicates that the deviations may be related to shortcomings in the force-field or experimental determination. The RMSE values compared to experiment are between 5.6 and 6.4 kJ mol⁻¹ and the Spearman correlation coefficients between 0.79 and 0.81 (bottom left panel in Fig. 5, Table I). Overall, the obtained $\Delta\Delta G_{\text{hyd}}$ values are again very similar for all schemes, and small differences should not be over interpreted. Relative to MBAR, the RMSE values are between 0.4 and 1.1 kJ mol⁻¹ and the Spearman correlation coefficients between 0.99 and 1.00 (bottom middle panel in Fig. 5, Table S3 in the supplementary material).

The agreement between the $\Delta\Delta G_{\text{CHCl}_3}$ values obtained from RE-EDS in GROMOS and the experimental values was better than for the hydration free energies. The RMSE values are between 4.8 and 5.6 kJ mol⁻¹ and the Spearman correlation coefficients between 0.42 and 0.65 (bottom right panel in Fig. 5, Table I).

c. Timings. The comparison of the total simulation time to obtain converged relative hydration free energies with RE-EDS (i.e., 376 ns for set C and 347 ns for set D with AT^{shift}) compared to the total simulation time for the MBAR results (i.e., 1442 ns for set C and 1339 ns for set D) highlights the high intrinsic sampling efficiency of RE-EDS (Table I). Note that the small variations in the required simulation time for the RE-EDS simulations in Table I stem from additional/fewer replicas due to a lower/higher lower bound for the *s*-values. A more detailed discussion on timings of RE-EDS calculations compared to other simulation methods (TI and MBAR) is provided in Ref. 22.

Based on these results, using a cutoff of 1.0 or 1.2 nm is appropriate for both considered sets of molecules. With the exception of the $\Delta\Delta G_{\text{CHCl}_3}^{\text{RE-EDS}}$ values using CG^{orig}, even a low cutoff of 0.8 nm leads to comparable accuracy. As the ΔG_{hyd} values calculated with MBAR and reported in the FreeSolv database were obtained with a cutoff of 1.2 nm for the electrostatic interactions,⁵¹ $R_{\text{RF}} = 1.2$ nm is the most appropriate choice to compare to $\Delta\Delta G_{\text{hyd}}^{\text{MBAR}}$. The results obtained with the different RF schemes achieve comparable accuracy within the uncertainty of the calculations. However, as the AT^{shift} scheme was shown to decrease cutoff artifacts for simulations with an atom-based cutoff significantly,⁴³ this is the most appropriate scheme to employ when using force fields that do not rely on charge groups.

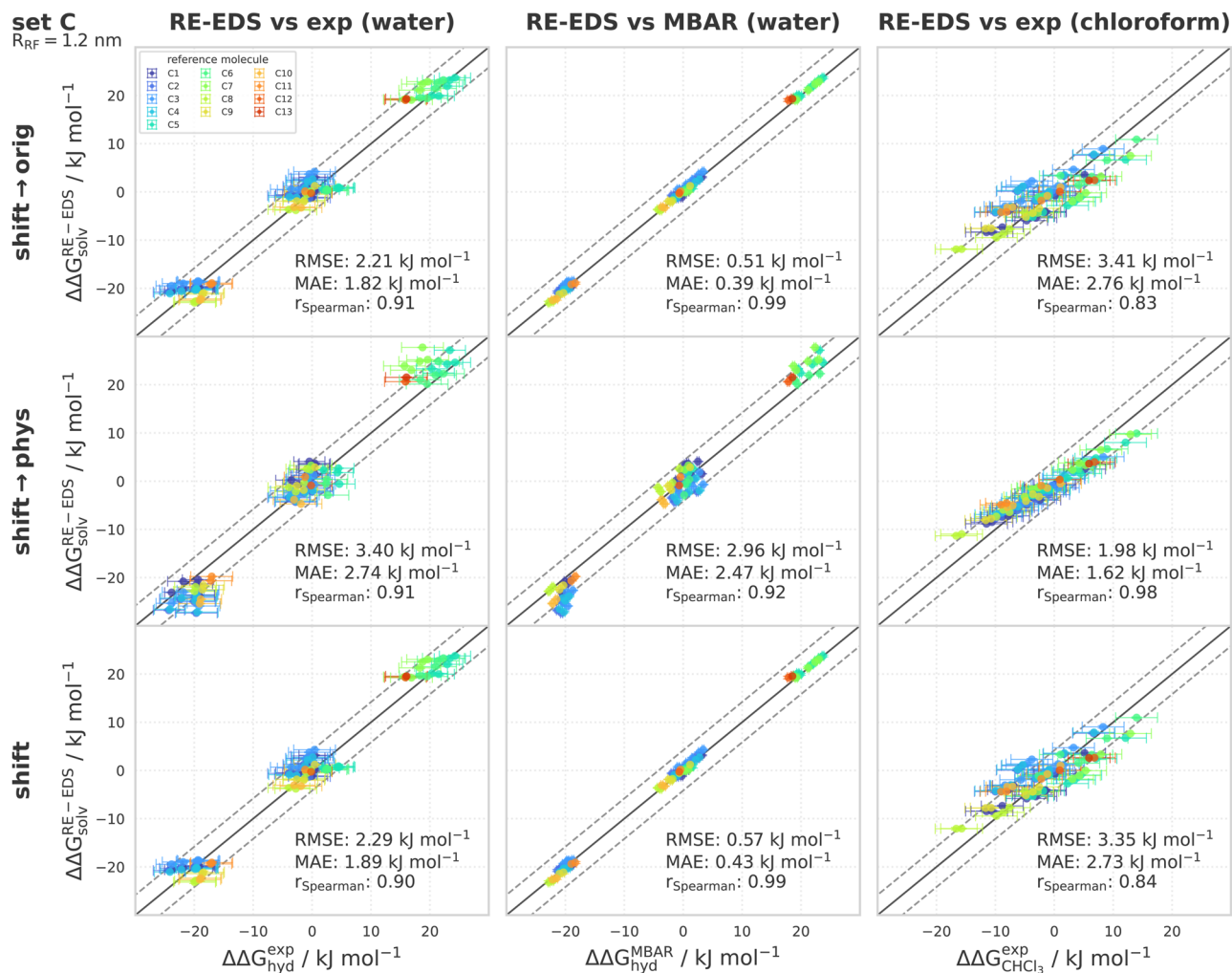


FIG. 4. Comparison of the relative solvation free energies of set C: $\Delta\Delta G_{\text{solv}}^{\text{RE-EDS}}$ obtained from RE-EDS calculations in GROMOS with $R_{\text{RF}} = 1.2 \text{ nm}$, propagated with the AT^{shift} scheme vs the experimental and calculated reference values. The three columns correspond to the comparison against $\Delta\Delta G_{\text{hyd}}^{\text{exp}}$ ^{50,51} (left), $\Delta\Delta G_{\text{hyd}}^{\text{MBAR}}$ ^{50,51} (middle), and $\Delta\Delta G_{\text{CHCl}_3}^{\text{exp}}$ ⁵² (right), respectively. The three rows correspond to using the corrected electrostatic potential energy $V^{\text{shift}\rightarrow\text{orig}}$ (top), $V^{\text{shift}\rightarrow\text{phys}}$ (middle), and the shifted electrostatic potential energy $V^{\text{ele},\text{shift}}$ (bottom), respectively. The gray diagonal lines correspond to perfect alignment within $\pm 4.184 \text{ kJ mol}^{-1}$ ($\pm 1 \text{ kcal mol}^{-1}$). The results obtained from RE-EDS were averaged over five repeats in each environment and the errors on the ΔG values correspond to the standard deviation over the five repeats. The error estimate of the ΔG values was calculated via Gaussian error propagation. The $\Delta\Delta G^i$ values are colored according to end-state i (i.e., the “reference molecule” for the calculation). The complete numerical values for all combinations of the three RF schemes and of the three cutoff distances are provided in Tables S4–S7, S13, and S14 in the [supplementary material](#). The corresponding plots are provided in Figs. S1–S3 and S7–S9 in the [supplementary material](#).

2. Free-energy differences from corrected energies

The $\Delta\Delta G$ values obtained from the RE-EDS calculations in GROMOS with AT^{shift} were compared to the values obtained with the “corrected” energies $V^{\text{shift}\rightarrow\text{orig}}$ and $V^{\text{shift}\rightarrow\text{phys}}$ [Eqs. (17) and (20)]. The systems were propagated with the AT^{shift} scheme, and the extra energy terms $V_i^{\text{extra},\text{orig}}$ and $V_i^{\text{extra},\text{phys}}$ were stored in the energy trajectory for all the end-states i .

a. Set C. For set C, the use of corrected end-state and reference-state electrostatic potential energies $V^{\text{shift}\rightarrow\text{orig}}$ to calculate

the relative hydration free energies resulted in negligible changes (left panel in Fig. 4, Table II). Using $V^{\text{shift}\rightarrow\text{phys}}$, on the other hand, significantly diminished the agreement with experimental values. The same trends were observed for the agreement with the values obtained from MBAR (middle panel in Fig. 4, Table S12 in the [supplementary material](#)). In the low permittivity environment of chloroform, on the other hand, using $V^{\text{shift}\rightarrow\text{phys}}$ to calculate the relative solvation free energies significantly increased the agreement with experimental reference values. At $R_{\text{RF}} = 1.2 \text{ nm}$, the RMSE was 2.0 kJ mol^{-1} compared to a RMSE of 3.4 kJ mol^{-1} when $V^{\text{ele},\text{shift}}$

TABLE I. Overview of statistical metrics (RMSE, MAE, Spearman correlation coefficient) as well as simulation time (t_{prep} and t_{prod}) for different RF schemes and cutoff distances for sets C and D. The uncertainties of the RMSE and MAE values were estimated from the distribution of RMSEs and MAEs when a random selection of up to 12 (set C) or 11 (set D) molecules was removed from the calculations (5000 repetitions). Top left: $\Delta\Delta G_{\text{hyd}}^{\text{RE-EDS}}$ vs $\Delta\Delta G_{\text{hyd}}^{\text{exp}}$ ^{50,51}. Top right: $\Delta\Delta G_{\text{hyd}}^{\text{MBAR}}$ ^{50,51} vs $\Delta\Delta G_{\text{hyd}}^{\text{exp}}$ ^{50,51}. For the MBAR calculations, the cutoff was 1.2 nm for the electrostatic interactions and 1.0 nm for the vdW interactions (with a switch at 0.9 nm and a long-range dispersion correction).⁵¹ Bottom left: $\Delta\Delta G_{\text{CHCl}_3}^{\text{RE-EDS}}$ vs $\Delta\Delta G_{\text{CHCl}_3}^{\text{exp}}$.⁵²

$\Delta\Delta G_{\text{hyd}}^{\text{RE-EDS}}$ vs $\Delta\Delta G_{\text{hyd}}^{\text{exp}}$						
Set	Scheme	Cutoff (nm)	RMSE (kJ mol ⁻¹)	MAE (kJ mol ⁻¹)	r_{Spearman}	t_{prep} (ns)
C	CG ^{orig}	0.8	2.2 ± 0.2	1.8 ± 0.2	0.89	309.2 67
		1.0	2.1 ± 0.2	1.7 ± 0.2	0.91	309.2 67
		1.2	2.2 ± 0.2	1.8 ± 0.2	0.91	309.2 67
		0.8	2.3 ± 0.2	1.9 ± 0.2	0.90	309.2 67
	AT ^{orig}	1.0	2.3 ± 0.2	1.9 ± 0.2	0.90	309.2 67
		1.2	2.2 ± 0.2	1.8 ± 0.2	0.91	309.2 67
		0.8	2.8 ± 0.2	2.3 ± 0.2	0.84	309.2 67
		1.0	2.4 ± 0.2	2.0 ± 0.2	0.89	309.2 67
	AT ^{shift}	1.2	2.3 ± 0.2	1.9 ± 0.2	0.90	309.2 67
		0.8	6.4 ± 0.6	5.4 ± 0.5	0.79	281 66
D	CG ^{orig}	1.0	6.3 ± 0.6	5.3 ± 0.5	0.80	286.2 68
		1.2	6.2 ± 0.7	5.2 ± 0.6	0.80	281 66
		0.8	5.8 ± 0.6	4.9 ± 0.5	0.81	281 66
		1.0	6.0 ± 0.6	5.0 ± 0.6	0.80	281 66
	AT ^{orig}	1.2	6.2 ± 0.6	5.2 ± 0.6	0.80	281 66
		0.8	5.6 ± 0.6	4.7 ± 0.6	0.81	281 66
		1.0	6.0 ± 0.6	5.0 ± 0.6	0.81	281 66
		1.2	6.1 ± 0.6	5.1 ± 0.6	0.81	281 66
	AT ^{shift}	0.8	5.6 ± 0.5	4.6 ± 0.5	0.59	234 57
		1.0	3.5 ± 0.3	2.9 ± 0.2	0.84	277.2 59
C	AT ^{orig}	1.2	3.4 ± 0.3	2.7 ± 0.3	0.84	277.2 59
		0.8	3.7 ± 0.3	3.1 ± 0.3	0.81	277.2 59
		1.0	3.4 ± 0.3	2.7 ± 0.2	0.84	277.2 59
		1.2	3.3 ± 0.3	2.7 ± 0.3	0.85	277.2 59
	AT ^{shift}	0.8	3.6 ± 0.3	3.0 ± 0.3	0.82	277.2 59
		1.0	3.4 ± 0.3	2.8 ± 0.3	0.84	277.2 59
		1.2	3.4 ± 0.3	2.7 ± 0.3	0.84	277.2 59
		0.8	5.6 ± 0.7	4.4 ± 0.7	0.42	207.8 56
D	CG ^{orig}	1.0	4.8 ± 0.5	4.0 ± 0.5	0.64	211 58
		1.2	4.9 ± 0.5	4.1 ± 0.4	0.64	211 58
		0.8	5.1 ± 0.5	4.2 ± 0.5	0.61	211 58
		1.0	5.0 ± 0.5	4.1 ± 0.4	0.64	211 58
	AT ^{orig}	1.2	4.9 ± 0.4	4.1 ± 0.4	0.64	211 58
		0.8	5.0 ± 0.5	4.2 ± 0.5	0.61	211 58
		1.0	5.1 ± 0.5	4.2 ± 0.5	0.63	211 58
		1.2	5.0 ± 0.5	4.1 ± 0.4	0.65	211 58

$\Delta\Delta G_{\text{CHCl}_3}^{\text{RE-EDS}}$ vs $\Delta\Delta G_{\text{CHCl}_3}^{\text{exp}}$						
Set	Scheme	Cutoff (nm)	RMSE (kJ mol ⁻¹)	MAE (kJ mol ⁻¹)	r_{Spearman}	t_{prod} (ns)
C	CG ^{orig}	0.8	5.6 ± 0.5	4.6 ± 0.5	0.59	234 57
		1.0	3.5 ± 0.3	2.9 ± 0.2	0.84	277.2 59
		1.2	3.4 ± 0.3	2.7 ± 0.3	0.84	277.2 59
		0.8	3.7 ± 0.3	3.1 ± 0.3	0.81	277.2 59
	AT ^{orig}	1.0	3.4 ± 0.3	2.7 ± 0.2	0.84	277.2 59
		1.2	3.3 ± 0.3	2.7 ± 0.3	0.85	277.2 59
		0.8	3.6 ± 0.3	3.0 ± 0.3	0.82	277.2 59
		1.0	3.4 ± 0.3	2.8 ± 0.3	0.84	277.2 59
	AT ^{shift}	1.2	3.4 ± 0.3	2.7 ± 0.3	0.84	277.2 59
		0.8	5.6 ± 0.7	4.4 ± 0.7	0.42	207.8 56
D	CG ^{orig}	1.0	4.8 ± 0.5	4.0 ± 0.5	0.64	211 58
		1.2	4.9 ± 0.5	4.1 ± 0.4	0.64	211 58
		0.8	5.1 ± 0.5	4.2 ± 0.5	0.61	211 58
		1.0	5.0 ± 0.5	4.1 ± 0.4	0.64	211 58
	AT ^{orig}	1.2	4.9 ± 0.4	4.1 ± 0.4	0.64	211 58
		0.8	5.0 ± 0.5	4.2 ± 0.5	0.61	211 58
		1.0	5.1 ± 0.5	4.2 ± 0.5	0.63	211 58
		1.2	5.0 ± 0.5	4.1 ± 0.4	0.65	211 58

TABLE I. (Continued.)

$\Delta\Delta G_{\text{hyd}}^{\text{MBAR}}$ vs $\Delta\Delta G_{\text{hyd}}^{\text{exp}}$				
Set	RMSE (kJ mol ⁻¹)	MAE (kJ mol ⁻¹)	r_{Spearman}	t_{prep} (ns)
C	1.9 ± 0.1	1.6 ± 0.1	0.93	42 1400
D	5.9 ± 0.6	4.9 ± 0.6	0.81	39 1300

was used directly. Using $V^{\text{shift} \rightarrow \text{orig}}$ had a negligible impact on the agreement with experiment (right panel in Fig. 4, Table II).

b. Set D. For set D, using $V^{\text{shift} \rightarrow \text{orig}}$ to calculate the $\Delta\Delta G_{\text{hyd}}$ values had again a negligible impact on the agreement with experiment, while using $V^{\text{shift} \rightarrow \text{phys}}$ slightly improved the reported metrics (e.g., at $R_{\text{RF}} = 1.2$ nm, the RMSE was 5.7 kJ mol⁻¹ compared to 6.1 kJ mol⁻¹, see the left panel in Fig. 5, Table II). The agreement with the MBAR results, on the other hand, significantly decreased when using $V^{\text{shift} \rightarrow \text{phys}}$, analogous to set C. Here, the RMSE was 2.3 kJ mol⁻¹ at $R_{\text{RF}} = 1.2$ nm compared to 0.5 kJ mol⁻¹ when using $V^{\text{ele}, \text{shift}}$ directly (middle panel in Fig. 5, Table S12 in the supplementary material). As for set C, the agreement with experiment for the relative solvation free energies in chloroform significantly improved upon using the corrected energies $V^{\text{shift} \rightarrow \text{phys}}$. For example, at $R_{\text{RF}} = 1.2$ nm, the RMSE was 3.6 kJ mol⁻¹ compared to 5.0 kJ mol⁻¹ (right panel in Fig. 5, Table II).

Based on these results, propagating a system with the electrostatic potential-energy term $V^{\text{ele}, \text{shift}}$ and using the corrected energy $V^{\text{shift} \rightarrow \text{phys}} = V^{\text{shift}} + V^{\text{extra, phys}}$ for analysis could potentially have a significantly positive effect on the accuracy of MD (free-energy) calculations. However, as the trend was not consistent across all systems, the observed improvements could be due to error cancellation effects and more investigations are needed before drawing a firm conclusion. In contrast, it is evident that using $V^{\text{shift} \rightarrow \text{orig}}$ does not improve the free-energy differences obtained based on GAFF topologies.

B. RE-EDS simulations in OpenMM

To validate the implementation of RE-EDS in OpenMM, the relative hydration free energies of sets A, C, and D were compared to the experimental reference values,^{50,51} the calculated values obtained with MBAR,^{50,51} as well as the values obtained with RE-EDS in GROMOS. Furthermore, the relative free energies in chloroform for sets C and D were compared to the experimental reference values,⁵² as well as the results obtained with RE-EDS in GROMOS. For the RE-EDS simulations in OpenMM, the AT^{shift} scheme with a cutoff of 1.2 nm was chosen for the electrostatic interactions.

For set A, there was excellent agreement between the $\Delta\Delta G_{\text{hyd}}$ values calculated with RE-EDS in OpenMM and in GROMOS. The RMSE and MAE were 0.2 kJ mol⁻¹ and the Spearman correlation coefficient was 1.00. According to the reported metrics, the agreement with experimental reference values was slightly better for the values obtained with RE-EDS in OpenMM

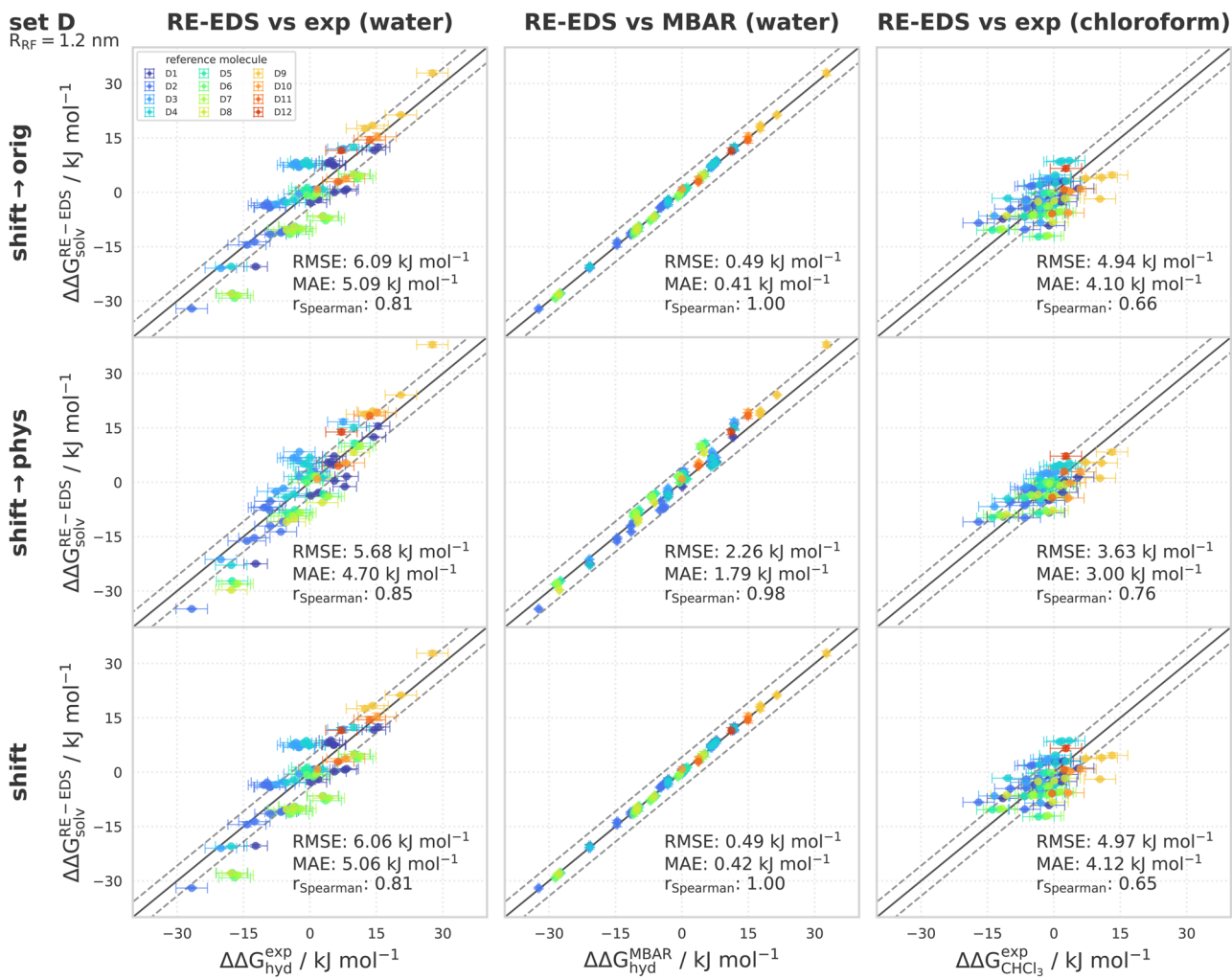


FIG. 5. Comparison of the relative solvation free energies of set D: $\Delta\Delta G_{\text{solv}}^{\text{RE-EDS}}$ obtained from RE-EDS calculations in GROMOS with $R_{RF} = 1.2 \text{ nm}$, propagated with the AT^{shift} scheme vs the experimental and calculated reference values. The three columns correspond to the comparison against $\Delta\Delta G_{\text{hyd}}^{\text{exp}}$ (left), $\Delta\Delta G_{\text{hyd}}^{\text{MBAR}}$ (middle), and $\Delta\Delta G_{\text{CHCl}_3}^{\text{exp}}$ (right), respectively. The three rows correspond to using the corrected electrostatic potential energy $V^{\text{shift} \rightarrow \text{orig}}$ (top), $V^{\text{shift} \rightarrow \text{phys}}$ (middle), and the shifted electrostatic potential energy $V^{\text{ele}, \text{shift}}$ (bottom), respectively. The gray diagonal lines correspond to perfect alignment within $\pm 4.184 \text{ kJ mol}^{-1}$ ($\pm 1 \text{ kcal mol}^{-1}$). The results obtained from RE-EDS were averaged over five repeats in each environment and the errors on the ΔG values correspond to the standard deviation over the five repeats. The error estimate of the $\Delta\Delta G$ values was calculated via Gaussian error propagation. The $\Delta\Delta G^i$ values are colored according to end-state i (i.e., the “reference molecule” for the calculation). The complete numerical values for all combinations of the three RF schemes and of the three cutoff distances are provided in Tables S8–S11, S15, and S16 in the [supplementary material](#). The corresponding plots are provided in Figs. S4–S6 and S10–S12 in the [supplementary material](#).

than with RE-EDS in GROMOS and with MBAR^{50,51} in GROMACS (left panel in Fig. 6, Table III).

Analogous to set A, the agreement between the $\Delta\Delta G_{\text{hyd}}$ values obtained from RE-EDS in GROMOS and in OpenMM was excellent for set C (top middle panel in Fig. 6). The RMSE and MAE values were 0.4 kJ mol^{-1} and the Spearman correlation coefficient was 0.99. Also here, the agreement with the experimental reference values was slightly better for the OpenMM results than the GROMOS ones (Table III). In chloroform, the agreement between the relative solvation free energies obtained with RE-EDS in GROMOS

and OpenMM was also excellent with an RMSE of 0.7 kJ mol^{-1} and a Spearman correlation coefficient of 0.98 (bottom middle panel in Fig. 6). The agreement with the experimental values was slightly better for the results obtained with OpenMM than with GROMOS (Table III).

Finally, similar observations were made for set D in water and chloroform, showing excellent agreement between the RE-EDS implementations in GROMOS and OpenMM (right panels in Fig. 6) and comparable results against experiment (Table III).

TABLE II. Overview of statistical metrics (RMSE, MAE, Spearman correlation coefficient) for RE-EDS simulations using the AT^{shift} scheme with and without corrected energy terms for sets C and D. The uncertainties of the RMSE and MAE values were estimated from the distribution of RMSEs and MAEs when a random selection of up to 12 (set C) or 11 (set D) molecules was removed from the calculations (5000 repetitions). Top: $\Delta\Delta G_{\text{hyd}}^{\text{RE-EDS}}$ vs $\Delta\Delta G_{\text{hyd}}^{\text{exp}}$ ^{50,51} Bottom: $\Delta\Delta G_{\text{CHCl}_3}^{\text{RE-EDS}}$ vs $\Delta\Delta G_{\text{CHCl}_3}^{\text{exp}}$.⁵²

$\Delta\Delta G_{\text{hyd}}^{\text{RE-EDS}}$ vs $\Delta\Delta G_{\text{hyd}}^{\text{exp}}$					
Set	V^{ele}	Cutoff (nm)	RMSE (kJ mol ⁻¹)	MAE (kJ mol ⁻¹)	r_{Spearman}
C	shift → orig	0.8	2.4 ± 0.2	1.9 ± 0.2	0.89
		1.0	2.2 ± 0.2	1.8 ± 0.2	0.91
		1.2	2.2 ± 0.2	1.8 ± 0.2	0.91
		0.8	3.5 ± 0.5	2.8 ± 0.4	0.90
	shift → phys	1.0	3.3 ± 0.4	2.7 ± 0.4	0.92
		1.2	3.4 ± 0.5	2.7 ± 0.4	0.91
		0.8	2.8 ± 0.2	2.3 ± 0.2	0.84
	shift	1.0	2.4 ± 0.2	2.0 ± 0.2	0.89
		1.2	2.3 ± 0.2	1.9 ± 0.2	0.90
D	shift → orig	0.8	5.8 ± 0.7	4.8 ± 0.5	0.81
		1.0	6.1 ± 0.6	5.1 ± 0.6	0.80
		1.2	6.1 ± 0.6	5.1 ± 0.6	0.81
		0.8	5.4 ± 0.6	4.4 ± 0.6	0.87
	shift → phys	1.0	5.5 ± 0.6	4.6 ± 0.6	0.85
		1.2	5.7 ± 0.5	4.7 ± 0.5	0.85
		0.8	5.6 ± 0.6	4.7 ± 0.6	0.81
	shift	1.0	6.0 ± 0.6	5.0 ± 0.6	0.81
		1.2	6.1 ± 0.6	5.1 ± 0.6	0.81
$\Delta\Delta G_{\text{CHCl}_3}^{\text{RE-EDS}}$ vs $\Delta\Delta G_{\text{CHCl}_3}^{\text{exp}}$					
Set	V^{ele}	Cutoff (nm)	RMSE (kJ mol ⁻¹)	MAE (kJ mol ⁻¹)	r_{Spearman}
C	shift → orig	0.8	3.8 ± 0.3	3.1 ± 0.2	0.80
		1.0	3.5 ± 0.3	2.9 ± 0.3	0.83
		1.2	3.4 ± 0.3	2.8 ± 0.2	0.83
		0.8	2.4 ± 0.3	1.9 ± 0.2	0.99
	shift → phys	1.0	2.0 ± 0.2	1.6 ± 0.2	0.99
		1.2	2.0 ± 0.2	1.6 ± 0.2	0.98
		0.8	3.6 ± 0.3	3.0 ± 0.3	0.82
	shift	1.0	3.4 ± 0.3	2.8 ± 0.3	0.84
		1.2	3.4 ± 0.3	2.7 ± 0.3	0.84
D	shift → orig	0.8	4.9 ± 0.5	4.1 ± 0.5	0.61
		1.0	5.0 ± 0.5	4.2 ± 0.4	0.63
		1.2	4.9 ± 0.5	4.1 ± 0.4	0.66
		0.8	3.6 ± 0.4	3.0 ± 0.3	0.75
	shift → phys	1.0	3.7 ± 0.3	3.1 ± 0.3	0.74
		1.2	3.6 ± 0.3	3.0 ± 0.3	0.76
		0.8	5.0 ± 0.5	4.2 ± 0.5	0.61
	shift	1.0	5.1 ± 0.5	4.2 ± 0.5	0.63
		1.2	5.0 ± 0.5	4.1 ± 0.4	0.65

RE-EDS in GROMOS vs OpenMM

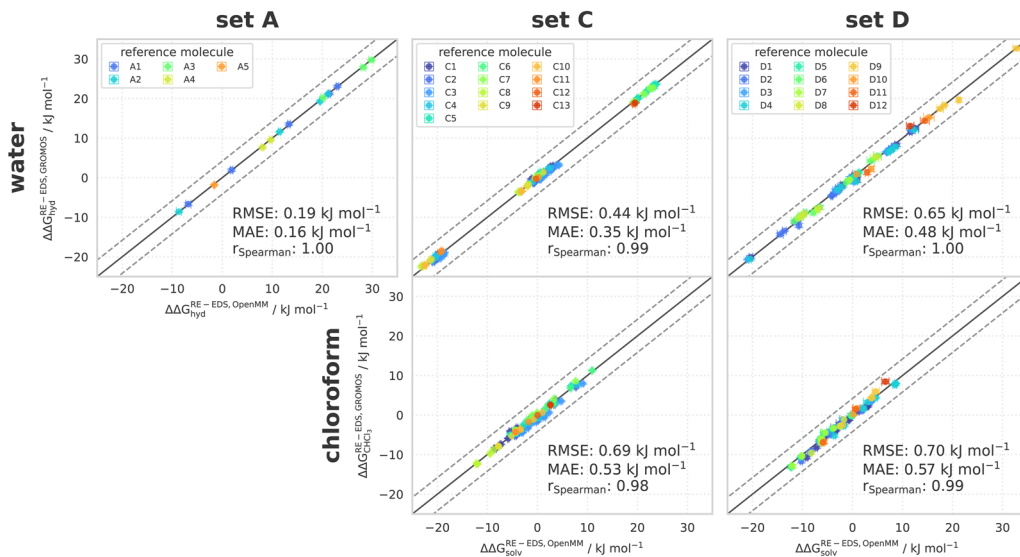


FIG. 6. Comparison of the relative solvation free energies in water of set A (left) and in water and chloroform of set C (middle) and D (right). Top: $\Delta\Delta G_{\text{hyd}}^{\text{RE-EDS,GROMOS}}$ obtained from RE-EDS calculations in GROMOS vs $\Delta\Delta G_{\text{hyd}}^{\text{RE-EDS,OpenMM}}$ obtained from RE-EDS calculations in OpenMM (both with the AT^{shift} scheme and $R_{\text{RF}} = 1.2 \text{ nm}$). Bottom: $\Delta\Delta G_{\text{CHCl}_3}^{\text{RE-EDS,GROMOS}}$ obtained from RE-EDS calculations in GROMOS vs $\Delta\Delta G_{\text{CHCl}_3}^{\text{RE-EDS,OpenMM}}$ obtained from RE-EDS calculations in OpenMM (both with the AT^{shift} scheme and $R_{\text{RF}} = 1.2 \text{ nm}$). The gray diagonal lines correspond to perfect alignment within $\pm 4.184 \text{ kJ mol}^{-1}$ ($\pm 1 \text{ kcal mol}^{-1}$). The results were averaged over five repeats in each environment and the errors on the ΔG values correspond to the standard deviation over the five repeats. The experimental errors of the free energies in chloroform were set to 0.6 kcal/mol (2.5104 kJ mol⁻¹), analogous to FreeSolv.^{50,51} The error estimate of the $\Delta\Delta G$ values was calculated via Gaussian error propagation. The $\Delta\Delta G^i$ values are colored according to end-state *i* (i.e., the “reference molecule” for the calculation). The numerical values are provided in Tables S17–S21 in the [supplementary material](#). All pairwise comparisons between the different simulation methods and the experimental results are shown in Figs. S13, S16, S19, S21, and S24 in the [supplementary material](#). Plots of the convergence of the free-energy calculations in each environment with RE-EDS in OpenMM and GROMOS are provided in Figs. S14, S15, S17, S18, S20, S22, S23, and S25 in the [supplementary material](#).

TABLE III. Overview of statistical metrics (RMSE, MAE, Spearman correlation coefficient) against experiment, as well as simulation time (t_{prep} and t_{prod}) for RE-EDS simulations in GROMOS and OpenMM (using the AT^{shift} scheme and $R_{\text{RF}} = 1.2 \text{ nm}$) and MBAR simulations in GROMACS as reported by FreeSolv.^{50,51} The uncertainties of the RMSE and MAE values were estimated from the distribution of RMSEs and MAEs when a random selection of up to 4 (set A), 12 (set C), or 11 (set D) molecules was removed from the calculations (5000 repetitions each).

Set	$\Delta\Delta G$	RMSE (kJ mol ⁻¹)	MAE (kJ mol ⁻¹)	r_{Spearman}	t_{prep} (ns)	t_{prod} (ns)
A	$\Delta\Delta G_{\text{hyd}}^{\text{RE-EDS,GROMOS}}$	2.6 ± 0.3	2.2 ± 0.3	0.97	89.3	13.5
	$\Delta\Delta G_{\text{hyd}}^{\text{RE-EDS,OpenMM}}$	2.5 ± 0.3	2.2 ± 0.3	0.97	89.3	13.5
	$\Delta\Delta G_{\text{hyd}}^{\text{MBAR}}$ ^{50,51}	3.1 ± 0.4	2.7 ± 0.3	0.98	18	600
C	$\Delta\Delta G_{\text{hyd}}^{\text{RE-EDS,GROMOS}}$	2.3 ± 0.2	1.9 ± 0.2	0.90	309.2	67
	$\Delta\Delta G_{\text{hyd}}^{\text{RE-EDS,OpenMM}}$	2.0 ± 0.1	1.6 ± 0.1	0.92	216.1	67
	$\Delta\Delta G_{\text{hyd}}^{\text{MBAR}}$ ^{50,51}	1.9 ± 0.1	1.6 ± 0.1	0.93	42	1400
	$\Delta\Delta G_{\text{CHCl}_3}^{\text{RE-EDS,GROMOS}}$	3.4 ± 0.3	2.7 ± 0.3	0.84	277.2	59
	$\Delta\Delta G_{\text{CHCl}_3}^{\text{RE-EDS,OpenMM}}$	2.9 ± 0.2	2.3 ± 0.2	0.90	177.1	59
D	$\Delta\Delta G_{\text{hyd}}^{\text{RE-EDS,GROMOS}}$	6.1 ± 0.6	5.1 ± 0.5	0.81	282.6	66
	$\Delta\Delta G_{\text{hyd}}^{\text{RE-EDS,OpenMM}}$	6.0 ± 0.6	5.0 ± 0.5	0.79	191.8	66
	$\Delta\Delta G_{\text{hyd}}^{\text{MBAR}}$ ^{50,51}	5.9 ± 0.6	4.9 ± 0.5	0.81	39	1300
	$\Delta\Delta G_{\text{CHCl}_3}^{\text{RE-EDS,GROMOS}}$	5.0 ± 0.5	4.1 ± 0.5	0.65	211	58
	$\Delta\Delta G_{\text{CHCl}_3}^{\text{RE-EDS,OpenMM}}$	5.0 ± 0.4	4.0 ± 0.4	0.66	153.8	58

Taken together, the results for the three sets A, C, and D demonstrate that the RE-EDS implementation in OpenMM can be used to calculate free-energy differences with a rigorously conservative scheme and a high sampling efficiency.

V. CONCLUSION AND OUTLOOK

To exploit the inherent sampling efficiency of RE-EDS with force fields using QM-derived charges and in MD engines without support for CG-based cutoff, we wanted to combine RE-EDS with the RF scheme including a shifting function that enables the use of AT-based cutoff in a rigorously conservative manner. For this, we first compared different RF schemes (CG^{orig} , AT^{orig} , and AT^{shift}) and cutoff values in the GROMOS MD engine using solvation free energies in water and chloroform as test properties. The results indicated that the AT^{shift} scheme can be used with RE-EDS by propagating the system with the electrostatic potential-energy term $V^{\text{ele, shift}}$.

Next, we implemented RE-EDS with the optimal RF scheme in the OpenMM MD engine. There were four main ingredients required for the implementation: (i) the definition of the nonbonded interactions based on V^{LJ} and $V^{\text{ele, shift}}$ via OpenMM's *CustomNonbondedForce* and *CustomBondForce*; (ii) the definition of atom–atom distance restraints via a *CustomBondForce* to prevent the molecules from drifting apart during the simulation; (iii) the EDS integration, i.e., the scaling of the nonbonded forces of the end-states based on the reference potential; and (iv) the simulation of independent replicas together with a replica-exchange criterion. The current proof-of-concept implementation is a simple Python3 module where the replicas are simulated serially. An implementation with improved parallelization is part of future work. The implementation in OpenMM was validated using solvation free energies in water and chloroform for three sets of molecules at $R_{\text{RF}} = 1.2 \text{ nm}$. The obtained $\Delta\Delta G_{\text{hyd}}$ and $\Delta\Delta G_{\text{CHCl}_3}$ values were compared to the analogous results obtained from RE-EDS in GROMOS, from MBAR in GROMACS (as reported by FreeSolv), and the experimental reference values. The agreement of the RE-EDS results obtained with the two MD engines was excellent, both for $\Delta\Delta G_{\text{hyd}}$ as well as $\Delta\Delta G_{\text{CHCl}_3}$, with RMSEs $\leq 0.7 \text{ kJ mol}^{-1}$. Similarly, good agreement was found for the results obtained with the state-of-the art method MBAR. Compared to experiment, the RE-EDS calculations in OpenMM provided a small but consistent improvement.

The developments presented in this study enable free-energy calculations with RE-EDS in GROMOS and OpenMM using force fields with QM-derived charges. This implementation will be used in the future to estimate binding free energies.

SUPPLEMENTARY MATERIAL

See the [supplementary material](#) for details about the datasets (C and D) and additional tables and figures for the comparison of RF schemes and cutoff values in GROMOS, the comparison of corrected electrostatic potential energies in GROMOS, and RE-EDS with OpenMM.

ACKNOWLEDGMENTS

The authors acknowledge financial support provided by the Swiss National Science Foundation (Grant Nos. 200021-178762 and

200021-175944). The authors thank Paul Katzberger for helpful discussions on replica exchange and OpenMM and Peter Eastman and John Chodera for helpful discussions regarding the future development of the RE-EDS implementation in OpenMM. The implementation of the RF correction via custom forces was inspired from a code snippet written by Alex Izvorski (<https://github.com/openmm/openmm/issues/3281>).

AUTHOR DECLARATIONS

Conflict of Interest

The authors have no conflicts to disclose.

Author Contributions

Salomé R. Rieder: Conceptualization (supporting); Investigation (lead); Methodology (lead); Software (lead); Validation (lead); Visualization (lead); Writing – original draft (lead). **Benjamin Ries:** Investigation (supporting); Methodology (supporting); Software (supporting); Writing – review & editing (supporting). **Alžbeta Kubincová:** Methodology (supporting); Writing – review & editing (supporting). **Candide Champion:** Methodology (supporting); Writing – review & editing (supporting). **Emilia P. Barros:** Methodology (supporting); Writing – review & editing (supporting). **Philippe H. Hünenberger:** Conceptualization (equal); Funding acquisition (equal); Methodology (equal); Project administration (equal); Supervision (equal); Writing – review & editing (equal). **Sereina Riniker:** Conceptualization (equal); Funding acquisition (equal); Methodology (equal); Project administration (equal); Supervision (equal); Writing – review & editing (equal).

DATA AVAILABILITY

The data that support the findings of this study are available within the article and its [supplementary material](#). The input files for the RE-EDS simulations can be found at https://github.com/rinikerlab/reeds/tree/main/examples/systems/shifted_reaction_field. The GROMOS software package and the GROMOS++ package of programs can be downloaded for free at <http://gromos.net/>, AmberTools at <https://ambermd.org/AmberTools.php>, and OpenMM at <https://openmm.org/>. The Python code for PyGromosTools and the RE-EDS pipeline is freely available at <https://github.com/rinikerlab>. The RE-EDS implementation using OpenMM can be found at https://github.com/rinikerlab/reeds/blob/main/reeds/openmm/reeds_openmm.py with example scripts provided at <https://github.com/rinikerlab/reeds/tree/main/examples/openmm>. The implementation of $V^{\text{ele, shift}}$ for single MD and (RE-)EDS simulations will be part of the next release of GROMOS.

REFERENCES

- ¹J. Michel, N. Foloppe, and J. W. Essex, “Rigorous free energy calculations in structure-based drug design,” *Mol. Inform.* **29**, 570–578 (2010).
- ²D. W. Borhani and D. E. Shaw, “The future of molecular dynamics simulations in drug discovery,” *J. Comput. Aided Mol. Des.* **26**, 15–26 (2012).

- ³M. De Vivo, M. Masetti, G. Bottegoni, and A. Cavalli, "Role of molecular dynamics and related methods in drug discovery," *J. Med. Chem.* **59**, 4035–4061 (2016).
- ⁴Z. Cournia, B. Allen, and W. Sherman, "Relative binding free energy calculations in drug discovery: Recent advances and practical considerations," *J. Chem. Inf. Model.* **57**, 2911–2937 (2017).
- ⁵B. J. Williams-Noonan, E. Yuriev, and D. K. Chalmers, "Free energy methods in drug design: Prospects of 'alchemical perturbation' in medicinal chemistry," *J. Med. Chem.* **61**, 638–649 (2018).
- ⁶K. A. Armacost, S. Riniker, and Z. Cournia, "Novel directions in free energy methods and applications," *J. Chem. Inf. Model.* **60**, 1–5 (2020).
- ⁷Z. Cournia, B. K. Allen, T. Beuming, D. A. Pearlman, B. K. Radak, and W. Sherman, "Rigorous free energy simulations in virtual screening," *J. Chem. Inf. Model.* **60**, 4153–4169 (2020).
- ⁸T.-S. Lee, B. K. Allen, T. J. Giese, Z. Guo, P. Li, C. Lin, T. D. McGee, Jr., D. A. Pearlman, B. K. Radak, Y. Tao, H.-C. Tsai, H. Xu, W. Sherman, and D. M. York, "Alchemical binding free energy calculations in AMBER20: Advances and best practices for drug discovery," *J. Chem. Inf. Model.* **60**, 5595–5623 (2020).
- ⁹L. F. Song and K. M. Merz, Jr., "Evolution of alchemical free energy methods in drug discovery," *J. Chem. Inf. Model.* **60**, 5308–5318 (2020).
- ¹⁰J. G. Kirkwood, "Statistical mechanics of fluid mixtures," *J. Chem. Phys.* **3**, 300–313 (1935).
- ¹¹R. W. Zwanzig, "High-temperature equation of state by a perturbation method. I. Nonpolar gases," *J. Chem. Phys.* **22**, 1420–1426 (1954).
- ¹²C. H. Bennett, "Efficient estimation of free energy differences from Monte Carlo data," *J. Comput. Phys.* **22**, 245–268 (1976).
- ¹³M. R. Shirts and J. D. Chodera, "Statistically optimal analysis of samples from multiple equilibrium states," *J. Chem. Phys.* **129**, 124105 (2008).
- ¹⁴J. L. Knight and C. L. Brooks III, "Multisite λ dynamics for simulated structure–activity relationship studies," *J. Chem. Theory Comput.* **7**, 2728–2739 (2011).
- ¹⁵E. P. Raman, T. J. Paul, R. L. Hayes, and C. L. Brooks III, "Automated, accurate, and scalable relative protein–ligand binding free-energy calculations using λ dynamics," *J. Chem. Theory Comput.* **16**, 7895–7914 (2020).
- ¹⁶R. L. Hayes, J. Buckner, and C. L. Brooks III, "BLaDE: A basic lambda dynamics engine for GPU-accelerated molecular dynamics free energy calculations," *J. Chem. Theory Comput.* **17**, 6799–6807 (2021).
- ¹⁷C. D. Christ and W. F. van Gunsteren, "Enveloping distribution sampling: A method to calculate free energy differences from a single simulation," *J. Chem. Phys.* **126**, 184110 (2007).
- ¹⁸C. D. Christ and W. F. van Gunsteren, "Multiple free energies from a single simulation: Extending enveloping distribution sampling to nonoverlapping phase-space distributions," *J. Chem. Phys.* **128**, 174112 (2008).
- ¹⁹D. Sidler, A. Schwaninger, and S. Riniker, "Replica exchange enveloping distribution sampling (RE-EDS): A robust method to estimate multiple free-energy differences from a single simulation," *J. Chem. Phys.* **145**, 154114 (2016).
- ²⁰D. Sidler, M. Cristófol-Clough, and S. Riniker, "Efficient round-trip time optimization for replica-exchange enveloping distribution sampling (RE-EDS)," *J. Chem. Theory Comput.* **13**, 3020–3030 (2017).
- ²¹B. Ries, K. Normak, R. G. Weiss, S. Rieder, E. de Barros, C. Champion, G. König, and S. Riniker, "Relative free-energy calculations for scaffold hopping-type transformations with an automated RE-EDS sampling procedure," *J. Comput. Aided Mol. Des.* **36**, 117–130 (2021).
- ²²S. R. Rieder, B. Ries, K. Schaller, C. Champion, E. P. Barros, P. H. Hünenberger, and S. Riniker, "Replica-exchange enveloping distribution sampling using generalized AMBER force-field topologies: Application to relative hydration free-energy calculations for large sets of molecules," *J. Chem. Inf. Model.* **62**, 3043–3056 (2022).
- ²³J. W. Perthold and C. Oostenbrink, "Accelerated enveloping distribution sampling: Enabling sampling of multiple end states while preserving local energy minima," *J. Phys. Chem. B* **122**, 5030–5037 (2018).
- ²⁴J. W. Perthold, D. Petrov, and C. Oostenbrink, "Toward automated free energy calculation with accelerated enveloping distribution sampling (A-EDS)," *J. Chem. Inf. Model.* **60**, 5395–5406 (2020).
- ²⁵N. Schmid, C. D. Christ, M. Christen, A. P. Eichenberger, and W. F. van Gunsteren, "Architecture, implementation and parallelization of the GROMOS software for biomolecular simulation," *Comput. Phys. Commun.* **183**, 890–903 (2012).
- ²⁶S. Riniker, C. D. Christ, N. Hansen, A. E. Mark, P. C. Nair, and W. F. van Gunsteren, "Comparison of enveloping distribution sampling and thermodynamic integration to calculate binding free energies of phenylethanolamine N-methyltransferase inhibitors," *J. Chem. Phys.* **135**, 024105 (2011).
- ²⁷U. H. E. Hansmann, "Parallel tempering algorithm for conformational studies of biological molecules," *Chem. Phys. Lett.* **281**, 140–150 (1997).
- ²⁸Y. Sugita, A. Kitao, and Y. Okamoto, "Multidimensional replica-exchange method for free-energy calculations," *J. Chem. Phys.* **113**, 6042–6051 (2000).
- ²⁹J. Lee, B. T. Miller, A. Damjanović, and B. R. Brooks, "Constant pH molecular dynamics in explicit solvent with enveloping distribution sampling and Hamiltonian exchange," *J. Chem. Theory Comput.* **10**, 2738–2750 (2014).
- ³⁰W. K. Hastings, "Monte Carlo sampling methods using Markov chains and their applications," *Biometrika* **57**, 97–109 (1970).
- ³¹B. Ries, S. Rieder, C. Rhiner, P. H. Hünenberger, and S. Riniker, "RestraintMaker: A graph-based approach to select distance restraints in free-energy calculations with dual topology," *J. Comput. Aided Mol. Des.* **36**, 175–192 (2022).
- ³²D. Chandler, J. D. Weeks, and H. C. Andersen, "Van der waals picture of liquids, solids, and phase transformations," *Science* **220**, 787–794 (1983).
- ³³C. L. Brooks III, "The influence of long-range force truncation on the thermodynamics of aqueous ionic solutions," *J. Chem. Phys.* **86**, 5156–5162 (1987).
- ³⁴H. Schreiber and O. Steinhauser, "Cutoff size does strongly influence molecular dynamics results on solvated polypeptides," *Biochemistry* **31**, 5856–5860 (1992).
- ³⁵E. Spohr, "Effect of electrostatic boundary conditions and system size on the interfacial properties of water and aqueous solutions," *J. Chem. Phys.* **107**, 6342–6348 (1997).
- ³⁶P. H. Hünenberger and W. F. van Gunsteren, "Alternative schemes for the inclusion of a reaction-field correction into molecular dynamics simulations: Influence on the simulated energetic, structural, and dielectric properties of liquid water," *J. Chem. Phys.* **108**, 6117–6134 (1998).
- ³⁷M. M. Reif, V. Kräutler, M. A. Kastenholz, X. Daura, and P. H. Hünenberger, "Molecular dynamics simulations of a reversibly folding β -heptapeptide in methanol: Influence of the treatment of long-range electrostatic interactions," *J. Phys. Chem. B* **113**, 3112–3128 (2009).
- ³⁸I. G. Tironi, R. Sperb, P. E. Smith, and W. F. van Gunsteren, "A generalized reaction field method for molecular dynamics simulations," *J. Chem. Phys.* **102**, 5451–5459 (1995).
- ³⁹P. P. Ewald, "Die Berechnung optischer und elektrostatischer Gitterpotentiale," *Ann. Phys.* **369**, 253–287 (1921).
- ⁴⁰R. Hockney and J. Eastwood, *Computer Simulation Using Particles* (CRC Press, 2021).
- ⁴¹T. Darden, D. York, and L. Pedersen, "Particle mesh Ewald: An $N \log(N)$ method for Ewald sums in large systems," *SoftwareX* **98**, 10089–10092 (1993).
- ⁴²U. Essmann, L. Perera, M. L. Berkowitz, T. Darden, H. Lee, and L. G. Pedersen, "A smooth particle mesh Ewald method," *J. Chem. Phys.* **103**, 8577–8593 (1995).
- ⁴³A. Kubincová, S. Riniker, and P. H. Hünenberger, "Reaction-field electrostatics in molecular dynamics simulations: Development of a conservative scheme compatible with an atomic cutoff," *Phys. Chem. Chem. Phys.* **22**, 26419–26437 (2020).
- ⁴⁴J. W. Cooley and J. W. Tukey, "An algorithm for the machine calculation of complex Fourier series," *Math. Comput.* **19**, 297–301 (1965).
- ⁴⁵P. H. Hünenberger, "Lattice-sum methods for computing electrostatic interactions in molecular simulations," in *Simulation and Theory of Electrostatic Interactions in Solution: Computational Chemistry, Biophysics, and Aqueous Solution*, edited by G. Hummer and L. R. Pratt (American Institute of Physics, New York, USA, 1999), Vol. 492.
- ⁴⁶J. P. Guthrie, "A blind challenge for computational solvation free energies: Introduction and overview," *J. Phys. Chem. B* **113**, 4501–4507 (2009).
- ⁴⁷S. Kashefogluha, M. P. Oliveira, S. R. Rieder, B. A. C. Horta, W. E. Acree, and P. H. Hünenberger, "Evaluating classical force fields against experimental cross-solvation free energies," *J. Chem. Theory Comput.* **16**, 7556–7580 (2020).

- ⁴⁸P. Eastman and V. Pande, "OpenMM: A hardware-independent framework for molecular simulations," *Comput. Sci. Eng.* **12**, 34–39 (2010).
- ⁴⁹P. Eastman, J. Swails, J. D. Chodera, R. T. McGibbon, Y. Zhao, K. A. Beauchamp, L.-P. Wang, A. C. Simmonett, M. P. Harrigan, C. D. Stern, R. P. Wiewiora, B. R. Brooks, and V. S. Pande, "OpenMM 7: Rapid development of high performance algorithms for molecular dynamics," *PLoS Comput. Biol.* **13**, e1005659 (2017).
- ⁵⁰D. L. Mobley and J. P. Guthrie, "FreeSolv: A database of experimental and calculated hydration free energies, with input files," *J. Comput. Aided Mol. Des.* **28**, 711–720 (2014).
- ⁵¹G. Duarte Ramos Matos, D. Y. Kyu, H. H. Loeffler, J. D. Chodera, M. R. Shirts, and D. L. Mobley, "Approaches for calculating solvation free energies and enthalpies demonstrated with an update of the FreeSolv database," *J. Chem. Eng. Data* **62**, 1559–1569 (2017).
- ⁵²A. V. Marenich, C. P. Kelly, J. D. Thompson, G. D. Hawkins, C. C. Chambers, D. J. Giesen, P. Winget, C. J. Cramer, and D. G. Truhlar, Minnesota solvation database, version 20, 2012.
- ⁵³W. F. van Gunsteren, S. R. Billeter, A. A. Eising, P. H. Hünenberger, P. Krüger, A. E. Mark, W. R. P. Scott, and I. G. Tironi, *Biomolecular Simulation: The GROMOS96 Manual and User Guide* (Vdf Hochschulverlag AG an der ETH Zürich, Zürich, Switzerland, 1996), pp. 1–1042.
- ⁵⁴S. Riniker, "Fixed-charge atomistic force fields for molecular dynamics simulations in the condensed phase: An overview," *J. Chem. Inf. Model.* **58**, 565–578 (2018).
- ⁵⁵See <http://gromos.net> for "The GROMOS software for (bio)molecular simulation, volume 2" (2021); accessed: 2022/05/05.
- ⁵⁶M. Bergdorf, C. Peter, and P. H. Hünenberger, "Influence of cut-off truncation and artificial periodicity of electrostatic interactions in molecular simulations of solvated ions: A continuum electrostatics study," *J. Chem. Phys.* **119**, 9129–9144 (2003).
- ⁵⁷M. Christen, P. H. Hünenberger, D. Bakowies, R. Baron, R. Bürgi, D. P. Geerke, T. N. Heinz, M. A. Kastenholz, V. Kräutler, C. Oostenbrink, C. Peter, D. Trzesniak, and W. F. van Gunsteren, "The GROMOS software for biomolecular simulation: GROMOS05," *J. Comput. Chem.* **26**, 1719–1751 (2005).
- ⁵⁸S. Riniker, A.-P. E. Kunz, and W. F. van Gunsteren, "On the calculation of the dielectric permittivity and relaxation of molecular models in the liquid phase," *J. Chem. Theory Comput.* **7**, 1469–1475 (2011).
- ⁵⁹A.-P. E. Kunz, J. R. Allison, D. P. Geerke, B. A. C. Horta, P. H. Hünenberger, S. Riniker, N. Schmid, and W. F. van Gunsteren, "New functionalities in the GROMOS biomolecular simulation software," *J. Comput. Chem.* **33**, 340–353 (2012).
- ⁶⁰J. Wang, R. M. Wolf, J. W. Caldwell, P. A. Kollman, and D. A. Case, "Development and testing of a general Amber force field," *J. Comput. Chem.* **25**, 1157–1174 (2004).
- ⁶¹D. A. Case, R. C. Walker, C. Cheatham, T. E. Simmerling, A. Roitberg, K. M. Merz, R. Luo, T. Darden, J. Wang, R. E. Duke, D. R. Roe, S. LeGrand, J. Swails, D. Cerutti, G. Monard, C. Sagui, J. Kaus, R. Betz, B. Madej, C. Lin, D. Mermelstein, P. Li, A. Onufriev, S. Izadi, R. M. Wolf, X. Wu, A. W. Götz, H. Gohlke, N. Homeyer, W. M. Botello-Smith, L. Xiao, T. Luchko, T. Giese, T. Lee, H. T. Nguyen, H. Nguyen, P. Janowski, I. Omelyan, A. Kovalenko, and P. A. Kollman, *AMBER Reference Manual* (University of California, San Francisco, 2016).
- ⁶²W. F. van Gunsteren, H. J. C. Berendsen, F. Colonna, D. Perahia, J. P. Hollenberg, and D. Lellouch, "On searching neighbors in computer simulations of macromolecular systems," *J. Comput. Chem.* **5**, 272–279 (1984).
- ⁶³C. Oostenbrink, A. Villa, A. E. Mark, and W. F. van Gunsteren, "A biomolecular force field based on the free enthalpy of hydration and solvation: The GROMOS force-field parameter sets 53A5 and 53A6," *J. Comput. Chem.* **25**, 1656–1676 (2004).
- ⁶⁴A. K. Malde, L. Zuo, M. Breeze, M. Stroet, D. Pogor, P. C. Nair, C. Oostenbrink, and A. E. Mark, "An automated force field topology builder (ATB) and repository: Version 1.0," *J. Chem. Theory Comput.* **7**, 4026–4037 (2011).
- ⁶⁵B. A. C. Horta, P. T. Merz, P. F. J. Fuchs, J. Dolenc, S. Riniker, and P. H. Hünenberger, "A GROMOS-compatible force field for small organic molecules in the condensed phase: The 2016H66 parameter set," *J. Chem. Theory Comput.* **12**, 3825–3850 (2016).
- ⁶⁶M. P. Oliveira, M. Andrey, S. R. Rieder, L. Kern, D. F. Hahn, S. Riniker, B. A. C. Horta, and P. H. Hünenberger, "Systematic optimization of a fragment-based force field against experimental pure-liquid properties considering large compound families: Application to saturated haloalkanes," *J. Chem. Theory Comput.* **16**, 7525–7555 (2020).
- ⁶⁷M. P. Oliveira and P. H. Hünenberger, "Systematic optimization of a fragment-based force field against experimental pure-liquid properties considering large compound families: Application to oxygen and nitrogen compounds," *Phys. Chem. Chem. Phys.* **23**, 17774–17793 (2021).
- ⁶⁸S. Canzar, M. El-Kebir, R. Pool, K. Elbassioni, A. K. Malde, A. E. Mark, D. P. Geerke, L. Stougie, and G. W. Klau, "Charge group partitioning in biomolecular simulation," *J. Comput. Biol.* **20**, 188–198 (2013).
- ⁶⁹A. Rahman and F. H. Stillinger, "Molecular dynamics study of liquid water," *J. Chem. Phys.* **55**, 3336–3359 (1971).
- ⁷⁰D. J. Adams, E. M. Adams, and G. J. Hills, "The computer simulation of polar liquids," *Mol. Phys.* **38**, 387–400 (1979).
- ⁷¹D. van der Spoel and P. J. van Maaren, "The origin of layer structure artifacts in simulations of liquid water," *J. Chem. Theory Comput.* **2**, 1–11 (2006).
- ⁷²V. Kräutler and P. H. Hünenberger, "Explicit-solvent molecular dynamics simulations of a DNA tetradecanucleotide duplex: Lattice-sum versus reaction-field electrostatics," *Mol. Simul.* **34**, 491–499 (2008).
- ⁷³B. Ni and A. Baumketner, "Effect of atom- and group-based truncations on biomolecules simulated with reaction-field electrostatics," *J. Mol. Model.* **17**, 2883–2893 (2011).
- ⁷⁴M. J. Abraham, T. Murtola, R. Schulz, S. Páll, J. C. Smith, B. Hess, and E. Lindahl, "GROMACS: High performance molecular simulations through multi-level parallelism from laptops to supercomputers," *SoftwareX* **1–2**, 19–25 (2015).
- ⁷⁵E. Lindahl, M. J. Abraham, B. Hess, and D. van der Spoel, GROMACS 2019.6 manual, 2020; accessed: 2020/05/19.
- ⁷⁶R. Salomon-Ferrer, D. A. Case, and R. C. Walker, "An overview of the Amber biomolecular simulation package," *Wiley Interdiscip. Rev.: Comput. Mol. Sci.* **3**, 198–210 (2013).
- ⁷⁷A. Glättli, X. Daura, and W. F. van Gunsteren, "Derivation of an improved simple point charge model for liquid water: SPC/A and SPC/L," *J. Chem. Phys.* **116**, 9811–9828 (2002).
- ⁷⁸G. J. Rocklin, D. L. Mobley, K. A. Dill, and P. H. Hünenberger, "Calculating the binding free energies of charged species based on explicit-solvent simulations employing lattice-sum methods: An accurate correction scheme for electrostatic finite-size effects," *J. Chem. Phys.* **139**, 184103 (2013).
- ⁷⁹M. M. Reif and C. Oostenbrink, "Net charge changes in the calculation of relative ligand-binding free energies via classical atomistic molecular dynamics simulations," *J. Comput. Chem.* **35**, 227–243 (2014).
- ⁸⁰C. Öhlknecht, J. W. Perthold, B. Lier, and C. Oostenbrink, "Charge-changing perturbations and path sampling via classical molecular dynamic simulations of simple guest-host systems," *J. Chem. Theory Comput.* **16**, 7721–7734 (2020).
- ⁸¹J. Swails, C. Hernandez, D. L. Mobley, H. Nguyen, L.-P. Wang, and P. Janowski, ParmEd, <https://github.com/ParmEd/ParmEd>, 2010; accessed: 2022/05/05.
- ⁸²S. Van Der Walt, S. C. Colbert, and G. Varoquaux, "The NumPy array: A structure for efficient numerical computation," *Comput. Sci. Eng.* **13**, 22–30 (2011).
- ⁸³W. McKinney, "Data structures for statistical computing in Python," *Proc. 9th Python Sci. Conf.* **445**, 56–61 (2010).
- ⁸⁴D. A. Pearlman and P. A. Kollman, "The overlooked bond-stretching contribution in free energy perturbation calculations," *J. Chem. Phys.* **94**, 4532–4545 (1991).
- ⁸⁵J. Gao, K. Kuczera, B. Tidor, and M. Karplus, "Hidden thermodynamics of mutant proteins: A molecular dynamics analysis," *Science* **244**, 1069–1072 (1989).
- ⁸⁶G. van Rossum and F. L. Drake, Python 3 reference manual, 2009.
- ⁸⁷B. Ries, S. R. Rieder, C. Champion, E. P. Barros, and S. Riniker, rinikerlab/reeds: An automatized RE-EDS sampling procedure (v1.0), 2021; accessed: 2022/05/05.
- ⁸⁸J. Wang, W. Wang, P. A. Kollman, and D. A. Case, "Automatic atom type and bond type perception in molecular mechanical calculations," *J. Mol. Graph. Model.* **25**, 247–260 (2006).

- ⁸⁹A. Jakalian, B. L. Bush, D. B. Jack, and C. I. Bayly, "Fast, efficient generation of high-quality atomic charges. AM1-BCC model: I. Method," *J. Comput. Chem.* **21**, 132–146 (2000).
- ⁹⁰A. Jakalian, D. B. Jack, and C. I. Bayly, "Fast, efficient generation of high-quality atomic charges. AM1-BCC model: II. Parameterization and validation," *J. Comput. Chem.* **23**, 1623–1641 (2002).
- ⁹¹A. P. Eichenberger, J. R. Allison, J. Dolenc, D. P. Geerke, B. A. C. Horta, K. Meier, C. Oostenbrink, N. Schmid, D. Steiner, D. Wang, and W. F. van Gunsteren, "The GROMOS++ software for the analysis of biomolecular simulation trajectories," *J. Chem. Theory Comput.* **7**, 3379–3390 (2011).
- ⁹²G. Landrum, P. Tosco, B. Kelley, S. Riniker, Ric, gedeck, R. Vianello, N. Schneider, A. Dalke, D. N, K. Eisuke, B. Cole, S. Turk, M. Swain, S. Alexander, D. Cosgrove, A. Vaucher, M. Wójcikowski, G. Jones, D. Probst, G. Godin, V. F. Scalfani, A. Pahl, B. Francois, J. L. Varjo, strels123, JP, Doliath Gavin, G. Sfora, and J. H. Jensen, rdkit/rdkit: 2021_03_2 (q1 2021) release, 2021; accessed: 2022/05/05.
- ⁹³W. F. van Gunsteren, gromos.net, <http://www.gromos.net/>, 2021; accessed: 2022/01/06.
- ⁹⁴W. L. Jorgensen, J. Chandrasekhar, J. D. Madura, R. W. Impey, and M. L. Klein, "Comparison of simple potential functions for simulating liquid water," *J. Chem. Phys.* **79**, 926–935 (1983).
- ⁹⁵I. G. Tironi and W. F. van Gunsteren, "A molecular dynamics simulation study of chloroform," *Mol. Phys.* **83**, 381–403 (1994).
- ⁹⁶D. R. Lide, *Handbook of Chemistry and Physics*, 88th ed. (CRC Press/Taylor and Francis, Boca Raton, FL, 2007–2008).
- ⁹⁷H. J. C. Berendsen, J. P. M. Postma, W. F. van Gunsteren, A. DiNola, and J. R. Haak, "Molecular dynamics with coupling to an external bath," *J. Chem. Phys.* **81**, 3684–3690 (1984).
- ⁹⁸J. Åqvist, P. Wennerström, M. Nervall, S. Bjelic, and B. O. Brandsdal, "Molecular dynamics simulations of water and biomolecules with a Monte Carlo constant pressure algorithm," *Chem. Phys. Lett.* **384**, 288–294 (2004).
- ⁹⁹J.-P. Ryckaert, G. Ciccotti, and H. J. C. Berendsen, "Numerical integration of the cartesian equations of motion of a system with constraints: Molecular dynamics of *n*-alkanes," *J. Comput. Phys.* **23**, 327–341 (1977).
- ¹⁰⁰S. Miyamoto and P. A. Kollman, "Settle: An analytical version of the SHAKE and RATTLE algorithm for rigid water models," *J. Comput. Chem.* **13**, 952–962 (1992).
- ¹⁰¹P. Eastman and V. S. Pande, "Constant constraint matrix approximation: A robust, parallelizable constraint method for molecular simulations," *J. Chem. Theory Comput.* **6**, 434–437 (2010).
- ¹⁰²M. R. Shirts, "Reweighting from the mixture distribution as a better way to describe the multistate Bennett acceptance ratio," [arXiv:1704.00891](https://arxiv.org/abs/1704.00891) (2017).
- ¹⁰³H. Bekker, H. J. C. Berendsen, E. J. Dijkstra, S. Achterop, R. van Drunen, D. van der Spoel, A. Sijbers, and H. Keegstra, "GROMACS: A parallel computer for molecular dynamics simulations," in *Physics Computing 92*, edited by R. A. DeGroot and J. Nadchal (World Scientific, Singapore, 1993), pp. 252–256.
- ¹⁰⁴M. T. Lehner, B. Ries, S. R. Rieder, and S. Riniker, rinikerlab/PyGromosTools: PyGromosTools_V2 (v2.0), 2021; accessed: 2022/05/05.
- ¹⁰⁵J. D. Hunter, "Matplotlib: A 2D graphics environment," *Comput. Sci. Eng.* **9**, 90–95 (2007).
- ¹⁰⁶F. Johansson, mpmath: A Python library for arbitrary-precision floating-point arithmetic (version 0.18), 2013; accessed: 2022/05/05.
- ¹⁰⁷P. Virtanen, R. Gommers, T. E. Oliphant, M. Haberland, T. Reddy, D. Cournapeau, E. Burovski, P. Peterson, W. Weckesser, J. Bright, S. J. van der Walt, M. Brett, J. Wilson, K. J. Millman, N. Mayorov, A. R. J. Nelson, E. Jones, R. Kern, E. Larson, C. J. Carey, İ. Polat, Y. Feng, E. W. Moore, J. VanderPlas, D. Laxalde, J. Perktold, R. Cimrman, I. Henriksen, E. A. Quintero, C. R. Harris, A. M. Archibald, A. H. Ribeiro, F. Pedregosa, P. van Mulbregt, A. Vijaykumar, A. P. Bardelli, A. Rothberg, A. Hilboll, A. Kloeckner, A. Scopatz, A. Lee, A. Rokem, C. N. Woods, C. Fulton, C. Masson, C. Häggström, C. Fitzgerald, D. A. Nicholson, D. R. Hagen, D. V. Pasechnik, E. Olivetti, E. Martin, E. Wieser, F. Silva, F. Lenders, F. Wilhelm, G. Young, G. A. Price, G.-L. Ingold, G. E. Allen, G. R. Lee, H. Audren, I. Probst, J. P. Dietrich, J. Silterra, J. T. Webber, J. Slavić, J. Nothman, J. Buchner, J. Kulick, J. L. Schönberger, J. V. de Miranda Cardoso, J. Reimer, J. Harrington, J. L. C. Rodríguez, J. Nunez-Iglesias, J. Kuczynski, K. Tritz, M. Thoma, M. Newville, M. Kümmeler, M. Bolingbroke, M. Tartre, M. Pak, N. J. Smith, N. Nowaczyk, N. Shebanov, O. Pavlyk, P. A. Brodtkorb, P. Lee, R. T. McGibbon, R. Feldbauer, S. Lewis, S. Tygier, S. Sievert, S. Vigna, S. Peterson, S. More, T. Pudlik, T. Oshima, T. J. Pingel, T. P. Robitaille, T. Spura, T. R. Jones, T. Cera, T. Leslie, T. Zito, T. Krauss, U. Upadhyay, Y. O. Halchenko, and Y. Vázquez-Baeza, "SciPy 1.0: Fundamental algorithms for scientific computing in Python," *Nat. Methods* **17**, 261–272 (2020).
- ¹⁰⁸M. L. Waskom, "seaborn: Statistical data visualization," *J. Open Source Software* **6**, 3021 (2021).
- ¹⁰⁹C. Spearman, "The proof and measurement of association between two things," *Am. J. Psychol.* **15**, 72–101 (1904).
- ¹¹⁰D. F. Hahn, C. I. Bayly, H. E. Bruce Macdonald, J. D. Chodera, A. S. J. S. Mey, D. L. Mobley, L. Perez Benito, C. E. M. Schindler, G. Tresadern, and G. L. Warren, "Best practices for constructing, preparing, and evaluating protein-ligand binding affinity benchmarks," [arXiv:2105.06222](https://arxiv.org/abs/2105.06222) (2021).